Reduced $CaCO_3$ flux to the seafloor and weaker bottom current speeds curtail benthic $CaCO_3$ dissolution over the 21st century

Olivier Sulpis[1*], Carolina O. Dufour[2], David S. Trossman[3], Andrea J. Fassbender[4], Brian K. Arbic[5], Bernard P. Boudreau[6], John P. Dunne[7] and Alfonso Mucci[1]

[1]GEOTOP and Earth and Planetary Sciences Department, McGill University, Montreal, QC, Canada
[2]Atmospheric and Oceanic Sciences Department, McGill University, Montreal, QC, Canada
[3]Institute of Computational Engineering and Sciences, The University of Texas at Austin, Austin, TX, USA
[4]Monterey Bay Aquarium Research Institute, Moss Landing, CA, USA
[5]Department of Earth and Environmental Sciences, University of Michigan, Ann Arbor, MI, USA
[6]Department of Oceanography, Dalhousie University, Halifax, NS, Canada
[7]Geophysical Fluid Dynamics Laboratory, National Oceanic and Atmospheric Administration, Princeton, NJ, USA

*correspondence: Department of Earth Sciences, Faculty of Geosciences, Utrecht University, Princetonlaan 8A, 3508 TA Utrecht, The Netherlands. Email: o.j.t.sulpis@uu.nl

Key points:

- Reduced $CaCO_3$ flux to the seafloor and weaker bottom current speeds curtail benthic $CaCO_3$ dissolution over the 21st century
- Modelled bottom currents underestimate current meter observations by up to 90%
- Under RCP8.5, the mean calcite compensation depth may rise by ~800 meters by the end of this century

Keywords: $CaCO_3$; dissolution; ocean acidification; RCP8.5; bottom currents

Abstract

Results from a range of Earth System and climate models of various resolution run under high-CO_2 emission scenarios challenge the paradigm that seafloor $CaCO_3$ dissolution will grow in extent and intensify as ocean acidification develops over the next century. Under the "business as usual", RCP8.5 scenario, $CaCO_3$ dissolution increases in some areas of the deep ocean, such as the eastern central Pacific Ocean, but is projected to decrease in the Northern Pacific and abyssal Atlantic Ocean by the year 2100. The flux of $CaCO_3$ to the seafloor and bottom-current speeds, both of which are expected to decrease globally through the 21st century, govern changes in benthic $CaCO_3$ dissolution rates over 53 and 31% of the dissolving seafloor, respectively. Below the calcite compensation depth (CCD), a reduced $CaCO_3$ flux to the $CaCO_3$-free seabed modulates the amount of $CaCO_3$ material dissolved at the sediment-water interface. Slower bottom-water circulation leads to thicker diffusive boundary layers above the sediment bed and a consequent stronger transport barrier to $CaCO_3$ dissolution. While all investigated models predict a weakening of bottom current speeds over most of the seafloor by the end of the 21st century, strong discrepancies exist in the magnitude of the predicted speeds. Overall, the poor performance of most models in reproducing modern bottom-water velocities and $CaCO_3$ rain rates coupled with the existence of large disparities in predicted bottom-water chemistry across models, hampers our ability to robustly estimate the magnitude and temporal evolution of anthropogenic $CaCO_3$ dissolution rates and the associated anthropogenic CO_2 neutralization.

Plain language summary

Carbon dioxide (CO_2), produced and released to the atmosphere by human activities, has been accumulating in the oceans for two centuries and will continue to do so well beyond the end of this century if emissions are not curbed. One direct consequence of CO_2 build-up in the ocean is the acidification of seawater. Calcite, a mineral secreted by many organisms living in the surface ocean to produce their shells and skeletons, covers a large part of the seafloor and acts as a natural antacid, neutralizing this excess CO_2. Model projections for the 21st century, under a "business as usual" scenario, reveal that seawater will become more corrosive to this mineral, but calcite dissolution at the seafloor will only increase slightly due to reductions in bottom-current speeds and in the amount of calcite particles delivered to the seafloor over that period. These results indicate that the neutralization of human-made CO_2 by calcite dissolution at the seafloor may take longer than previously anticipated.

1. Introduction

Anthropogenic carbon dioxide (CO_2) has been accumulating in the atmosphere since the beginning of the industrial era and, according to projections of future emissions, will continue to do so well beyond the end of this century [*Collins et al*., 2013; *Meinshausen et al*., 2011]. The global, mean atmospheric CO_2 concentration was ~280 parts per million (ppm) in 1750 [*Joos and Spahni*, 2008], reached 405 ppm in 2017 [*Dlugokencky and Tans*, 2018], and may exceed 1000 ppm by 2100 according to the "business as usual" Representative Concentration Pathway 8.5 (RCP8.5, *van Vuuren et al*. [2011]), a high-CO_2 emission scenario in which no specific climate mitigation action is taken [*Riahi et al*., 2011]. Each year, about 25% of the anthropogenic carbon emitted into the atmosphere is absorbed by the ocean [*Le Quéré et al*., 2018]. The absorption of CO_2 in seawater leads to a measurable pH decrease which, in turn, reduces the carbonate ion (CO_3^{2-}) concentration and lowers the saturation state of seawater with respect to calcium carbonate minerals ($CaCO_3$, e.g., calcite or aragonite), favouring their dissolution and impeding their precipitation [*Mackenzie and Andersson*, 2013]. These conditions are expected to intensify over the next centuries [*Caldeira and Wickett*, 2003; *Orr et al*., 2005; *Boudreau et al*., 2010b; *Boudreau et al*., 2018]. Recent research has indicated that the rate of anthropogenic carbon release is higher than during any other comparable event over at least the past 66 million years, highlighting the exceptional nature and rate of ongoing acidification [*Zeebe et al*., 2016]. It is critical that scientists and policy makers obtain accurate estimates of the timescales over which marine ecosystems will be impacted by this anthropogenic ocean acidification.

Two hypothetical pathways can be considered for the evolution of ocean acidification in a high-CO_2 world. In a poorly chemically-buffered ocean, CO_2 accumulation and the resulting seawater-pH decline are rapid, leading to runaway ocean acidification. In contrast, a well-buffered ocean can slow down the pH change through negative feedback mechanisms, whose kinetics then control the ocean recovery time towards its pre-acidification state once anthropogenic CO_2 emissions are curbed. One of these feedback mechanisms, the dissolution of marine $CaCO_3$ minerals, is thought to be the major sink for anthropogenic CO_2 on the time scale of decades to millennia [*Archer et al*., 2009; *Ridgwell and Hargreaves*, 2007] and is described by the overall reaction:

$$CaCO_3 + CO_2 + H_2O \leftrightarrow 2HCO_3^- + Ca^{2+} \quad (1)$$

Modern $CaCO_3$-rich sediments (> 30 % of the sediment dry weight) cover a third of the seafloor [*Dutkiewicz et al*., 2015; *Morse and Mackenzie*, 1990]. The distribution and $CaCO_3$ content of sediment are a function of the $CaCO_3$ production and export from the surface ocean, dilution of sedimentary $CaCO_3$ by authigenic and siliciclastic materials, and, most importantly, in-situ dissolution, which is a function of the saturation state of overlying waters with respect to $CaCO_3$. The latter is defined as:

$$\Omega = \frac{[Ca^{2+}]_{SW}[CO_3^{2-}]_{SW}}{K_{sp}^*} \quad (2)$$

where the square brackets indicate total concentrations in seawater in mol kg^{-1} and K_{sp}* is the stoichiometric solubility constant of the mineral of interest ($mol^2\ kg^{-2}$) at in-situ temperature, pressure, and salinity [*Millero*, 1995; *Mucci*, 1983]. If Ω is lower than 1, seawater is

undersaturated with respect to the $CaCO_3$ phase of interest (e.g., calcite or aragonite), which should dissolve if present. Although biogenic aragonite, calcite, and magnesian calcites dominate in the marine environment, only calcite and low magnesian-calcite phases ($MgCO_3$ < 4 % by mole) persist in deep-sea sediments [*Morse et al*., 2007]. As ocean acidification intensifies, the area of the seafloor covered by undersaturated waters will increase, and more dissolution of $CaCO_3$ minerals at the seafloor is expected [*Archer et al*., 2009; *Ridgwell and Hargreaves*, 2007; *Boudreau et al*., 2010a; *Alexander et al*., 2015]. It is this additional dissolution that neutralizes excess CO_2 and allows projections for the ocean to return to its pre-acidification state on a multi-millennial timescale after anthropogenic emissions are curbed [*Ciais et al*. 2013; *Boudreau et al.*, 2018].

Currently, 55 % of the anthropogenic CO_2 in the ocean is stored in the top 100 m of the water column, while the deep-ocean reservoir (i.e., below ~1000 m), which represents 76% of the ocean volume, contains only 4% of the anthropogenic CO_2 (from the data of *Khatiwala et al*. [2009]). Through the advection of anthropogenic CO_2-rich surface waters to the deep ocean (see, e.g., *MacGilchrist et al.*, 2019), additional anthropogenic CO_2 will invade the deep sea as CO_2 emissions continue throughout and beyond the 21st century. Whereas most research to date has focused on quantifying anthropogenic CO_2 invasion in the framework of global carbon budget considerations (e.g., *Anderson et al*. [1998]; *Khatiwala et al*. [2009]) or across targeted surface/intermediate waters (e.g., *Bates et al*. [2012]; *Carter et al*. [2017]), the penetration of anthropogenic CO_2 to the abyssal ocean and its impact on pH has not been extensively modeled or monitored. An accurate characterization of bottom-water chemistry and ocean currents is needed to assess the response of carbonate-rich sediments at the seafloor to anthropogenic acidification. Measurable amounts (i.e., > 4 µmol kg^{-1}) of anthropogenic CO_2 have been reported in the bottom waters of the Atlantic [*Chen*, 1982; *Körtzinger et al*., 1998; *Lauvset et al*., 2016; *McNeil et al*., 2003; *Perez et al*., 2018; *Wanninkhof et al*., 2013; *Woosley et al*., 2016], Pacific [*Sabine et al*., 2002], Arctic [*Vázquez-Rodríguez et al*., 2009] and Southern [*Chen*, 1982; *Lauvset et al*., 2016] Oceans.

In a recent study, *Sulpis et al*. [2018] showed that anthropogenic bottom-water acidification is now sufficiently advanced to trigger significant sedimentary calcite dissolution in the north-western Atlantic and the southern extents of the Atlantic, Pacific and Indian Oceans. Here, we use a diversity of Earth System and climate models to test the premise that over the next century, seafloor calcite dissolution will grow in extent and intensity as acidification persists. To do so, we estimate how global anthropogenic dissolution fluxes at the seafloor will evolve between 2006 and 2100. Subsequently, we test the dependency of benthic dissolution rates to various variables, such as the bottom-water dissolved inorganic carbon concentration and current velocities. Finally, we discuss the need for specific observational constraints to improve relevant model parameterizations.

2. Materials and methods

2.1. Models and data

Seawater chemical variables spanning the period 2006 to 2100 were extracted from the RCP8.5 simulations of three different models from the Coupled Model Intercomparison Project Phase 5 (CMIP5): the Global Coupled Climate-Carbon Earth System Model ESM2M [*Dunne et*

al., 2012; *Dunne et al*., 2013] developed at the Geophysical Fluid Dynamics Laboratory (GFDL) at Princeton, the IPSL-CM5A Medium Resolution Earth System Model [*Dufresne et al*., 2013] developed at the Institut Pierre Simon Laplace (IPSL), and the Hadley Global Environment Model 2 – Carbon Cycle (HadGEM2) [*Bellouin et al*., 2007; *Collins et al*., 2011] developed at the UK Met Office Hadley Centre. Although numerous other CMIP5 models exist, we chose to limit our analysis to these three CMIP5 models for consistency, as they are the only CMIP5 models for which all the bottom-water variables of interest were available. We used annual averages of total alkalinity (*TA*), dissolved inorganic carbon (*DIC*), in-situ temperature (*T*), practical salinity (S_P), dissolved inorganic silica concentration ([*dSi*]), soluble reactive phosphate concentration ([*SRP*]), sinking calcite flux (*F*), and seawater (near-)bottom velocity (*U*). The variable [*SRP*] was not available for the HADGEM2C-CC simulation and set at 2 μmol kg^{-1} based on version 2 Global Ocean Data Analysis Project data [*Lauvset et al*., 2016]. All model outputs were horizontally re-gridded onto the 1º x 1º grid of the World Ocean Atlas. For latitude-longitude coordinate, the deepest layer of the model was considered to be representative of bottom waters. For each model, the bottom-water carbonate ion concentration ($[CO_3^{2-}]_{SW}$) was computed using the MATLAB version of the CO2SYS algorithm [*Pierrot et al*., 2006; *van Heuven et al*., 2011], based on bottom-water *TA*, *DIC*, *T*, S_P, [*dSi*] and [*SRP*], using the carbonic acid dissociation constants (K_1^* and K_2^*) from *Lueker et al*. [2000] and the HSO_4^- dissociation constant from *Dickson* [1990]. We propagated errors in inorganic carbon chemistry according to *Orr et al*. [2018]. In-situ temperature and seawater density were computed using the MATLAB version of the GSW Oceanographic Toolbox [*McDougall and Barker*, 2011].

2.2. $CaCO_3$ dissolution rate calculation

As the salinity of the deep-ocean is nearly invariant and the seawater calcium concentration ($[Ca^{2+}]_{SW}$) is practically conservative (i.e., $[Ca^{2+}]_{SW} = f(S_P)$), the saturation state of the deep-ocean with respect to calcite, Ω_C, see Eq. (2), can be represented simply by $[CO_3^{2-}]_{SW}/[CO_3^{2-}]_{eq}$, where $[CO_3^{2-}]_{eq}$ is the seawater carbonate ion concentration at equilibrium with calcite. $[CO_3^{2-}]_{eq}$ was estimated from the equations presented in *Boudreau et al*. [2010b], using $[Ca^{2+}]$ computed from S_P following *Riley and Tongudai* [1967] and the calcite stoichiometric solubility constant (K_{sp}^*) at in-situ *T*, S_P [*Mucci*, 1983] and pressure (*P*; *Millero* [1995]).

The depth below which seawater becomes undersaturated with respect to calcite (i.e., $\Omega_C < 1$ or $[CO_3^{2-}]_{SW} < [CO_3^{2-}]_{eq}$), is referred to as the calcite saturation depth (*CSD*). For each model, the *CSD* was computed for each year from 2006 to 2100 using seawater density, $[Ca^{2+}]_{SW}$, $[CO_3^{2-}]_{SW}$, K_{sp}^* and the equations of *Boudreau et al*. [2010b]. Below the *CSD*, seawater is undersaturated with respect to calcite, and dissolution should, according to classical chemical kinetics theory, occur at a rate determined by the slowest step of the overall reaction (Eq. (1)), [*Morse and Arvidson*, 2002; *Naviaux et al*., 2019]. The slowest step or "kinetic barrier" controlling the rate of calcite dissolution at the seafloor is either the transport of molecular reactants and products across the diffusive boundary layer (DBL; *Schlichting* [1979]) at the sediment-water interface (typically a few hundred micrometers to a few millimeters-thick for deep-sea conditions; *Sulpis et al. [2018]*), or processes within the sediment such as molecular diffusion through the porewaters and reactions at mineral grain surfaces [*Boudreau*, 2013; *Boudreau and Guinasso*, 1982; *Sulpis et al*., 2017]. In the first case, the dissolution reaction is termed "water-side transport-controlled" and is strongly dependent on the current speed (*U*) of

the overlying waters [*Boudreau and Jørgensen*, 2001; *Dade*, 1993; *Steinberger and Hondzo*, 1999]. Fast bottom currents flatten the DBL and reduce the time necessary for reactants and reaction products to cross the DBL, enhancing the dissolution rate. Conversely, slow bottom-water currents thicken the DBL and impede the dissolution reaction. When processes within the sediment control the dissolution rate, the reaction is termed "sediment-side controlled" and is independent of the overlying water current speed. Currently, calcite dissolution is water-side transport controlled over most of the seafloor, but switches to sediment-side control in areas where sediments are calcite-poor [*Boudreau*, 2013; *Sulpis et al*., 2018]. Under this formalism, the dissolution rate is expressed as the product of an overall mass transfer coefficient and a concentration gradient, i.e., the deficit in CO_3^{2-} that drives the dissolution reaction.

$$r = k^*\left([CO_3^{2-}]_{eq} - [CO_3^{2-}]_{SW}\right) \quad (3)$$

where k^* is the CO_3^{2-} overall mass transfer coefficient (m a^{-1}), i.e.,

$$k^* = (k_S\beta)(k_S + \beta)^{-1} \quad (4)$$

where k_s is the sediment-side CO_3^{2-} mass transfer coefficient (m a^{-1}) and β is the water-side (DBL) CO_3^{2-} mass transfer coefficient (m a^{-1}).

The Calcite Compensation Depth (*CCD*) is the depth at which the calcite dissolution rate at the sediment-water interface equals the sinking flux of calcite delivered to the seafloor, referred to as the rain rate (F; *Bramlette* [1961]; *Edmond* [1974]). At steady state (e.g., preindustrial conditions), sediments are calcite-free below the *CCD*. Since the beginning of the industrial revolution, as anthropogenic CO_2 spreads through the deep sea, the oceans are no longer at a steady state, and both the *CCD* and *CSD* have been shoaling [*Boudreau et al*., 2010a; *Feely et al*., 2002; *Sulpis et al*., 2018]. As the *CCD* shoals, calcitic particles reaching sediments between the rising *CCD* and the preindustrial *CCD* dissolve completely at the sediment-water interface, but the underlying sediments, although now sitting below the *CCD*, will not become calcite-free for several tens of thousands of years, far beyond the time scale over which this study is focusing [*Boudreau and Luo*, 2017]. Below the preindustrial *CCD*, calcite does not accumulate in sediments because F is compensated entirely by dissolution. Thus, below the preindustrial *CCD*:

$$r = F. \quad (5)$$

For sediments between the preindustrial *CCD* and the rising *CCD*, the net dissolution rate is given by the sum of the carbonate rain rate and the dissolution rate of sediments previously deposited - the sum of Eqs. (3) and (5):

$$r = F + k^*\left([CO_3^{2-}]_{eq} - [CO_3^{2-}]_{SW}\right). \quad (6)$$

where F, k^*, $[CO_3^{2-}]_{eq}$ and $[CO_3^{2-}]_{SW}$ all vary in time. Above the contemporary *CCD*, the rate is computed using Eq. (3). Here, we use the preindustrial *CCD* values from *Sulpis et al*. [2018], which are based on measured $CaCO_3$ sediment contents, and initially set the 2006 *CCD* values to the present-day *CCD* values computed by *Sulpis et al*. [2018]. For each CMIP5 model, the *CCD* is subsequently allowed to move freely throughout the 21st century as the simulated seawater chemistry (i.e., $[CO_3^{2-}]_{SW}$), F and k^* evolve in time according to the equations described in *Boudreau et al*. [2010b]. Because the initial *CCD* values were computed from basin-averaged sediment-$CaCO_3$ content profiles (see *Sulpis et al*. [2018]), *CCD* predictions are only relevant

where the sediment-$CaCO_3$ distribution is controlled by vertical dissolution/deposition fluxes rather than lateral accumulation (i.e., $CaCO_3$ from turbidites or rivers). As the Southern and Arctic Oceans appear to fall in the category of lateral-transport dominated regions, and due to the lack of data in these regions, we exclude the Southern and Arctic Oceans (below 60 °S and above 60 °N, respectively) and the seafloor shallower than 300 m from our analysis. F, the calcite rain rate, was taken as the deepest simulated sinking calcite flux, expressed in mol m^{-2} a^{-1}, which we assume to be representative of the calcite flux reaching the seafloor.

β (see Eq. 4) was derived from the in-situ diffusion coefficient of CO_3^{2-} [*Zeebe*, 2011], the in-situ molecular kinematic viscosity of seawater and bottom speeds (U) for each model, using the equations presented in *Sulpis et al*. [2018]. U was computed as the sum of TPXO9.1 tidal velocities [*Egbert and Erofeeva*, 2002] (downloaded from http://volkov.oce.orst.edu/tides/ and horizontally re-gridded onto the 1º x 1º grid of the World Ocean Atlas) and annual averages of the resolved horizontal velocities in the deepest layer of each CMIP5 model under the RCP8.5 scenario. Whereas model-resolved velocities change through time, as predicted by each CMIP5 model, TPXO9.1 tidal velocities were assumed constant, given that the effect of climate variability on tidal currents is negligible [*Saynisch et al*., 2016]. U does not include parameterized velocities, such as those arising from the Gent and McWilliams scheme that most models use (see *Gent and McWilliams* [1990]; *Griffies* [1998]), because these velocities were not available in the model output. The role of subgrid-scale processes will be discussed in section 4.2. The resulting β distribution is shown in Fig. S1. Since β is dependent on seawater viscosity, it is impacted by variations of seawater T and S_P. β was allowed to evolve as a function of U, T and S_P between 2006 and 2100, and the impacts of this varying β on the dissolution rates were quantified. k_S, the sediment-side mass transfer coefficient, was computed from the $CaCO_3$ content of the sediments, taken from *Sulpis et al*. [2018], and set constant throughout the analysis timeframe. The resulting end-of-the-century k_S and the overall mass transfer coefficient, k^*, computed from Eq. (4), are shown in Fig. S1.

2.3. Bottom currents across models

In order to accurately estimate the response of the seafloor to future climate changes, a reliable representation and projection of bottom-current speeds is required. To evaluate the accuracy of the model-predicted bottom-current speeds, the non-tidal component of these speeds were compared to a new compilation of current meter data. The evolution of bottom currents throughout the 21st century were also compared between different coarse resolution models (~1° x ~1°) under RCP8.5 without tides. The current-speed spread between these models is hereafter termed the CMIP5-intermodel spread. In addition, to evaluate the impact of model horizontal resolution on the representation of bottom-current speeds, output of a suite of three climate models of different resolution (the CM2-O suite) were compared. The CM2-O suite includes CM2.6 [*Griffies et al*., 2015; *Winton et al*., 2014], which uses a 1/10th degree horizontal resolution, CM2.5 [*Delworth et al*., 2012], with a 1/4th degree horizontal resolution, and CM2-1deg [*Griffies et al*., 2015], with a 1 degree horizontal resolution. The CM2-O models were run under an atmospheric partial pressure of CO_2 (pCO_2) increase of 1% per year for 70 years starting at 286 ppm. This idealized CO_2 concentration scenario is similar to the RCP8.5 scenario used in the three CMIP5 models investigated in this study. Finally, we also used four simulations from the HYbrid Coordinate Ocean Model (HYCOM; *Trossman et al*. [2016]; an

ocean-sea ice model forced with atmospheric reanalyses - note that these simulations are of the present-day ocean only). Two of the HYCOM simulations were run in a $1/12^{th}$ degree configuration, and two were run in a $1/25^{th}$ degree configuration, with each configuration comprising one simulation that included a parameterized topographic internal lee wave drag, and another simulation without it, as described in *Trossman et al*. [2016]. Here, "Wave drag" refers to the momentum sink associated with the generation of internal lee waves, and accounts for a breaking effect when the geostrophic flow impinges upon rough topography, based on the theory of *Garner* [2005] and applied in *Trossman et al*. [2013]. Analogous to the CMIP5 models, neither the CM2-O models, nor HYCOM currently include tides.

The current-meter dataset contains measurements described by *Trossman et al*. [2016] and *Luecke et al.* [2017]. In order to remove tidal currents from the measurements, a low-pass filter was applied to each current-meter record. Only records containing a minimum of 105 days of observations were considered, following *Timko et al.* [2013]. At each location, measurements within 500 meters of the seafloor were averaged and considered to be representative of bottom currents, for comparison with bottom-current values simulated by models. We chose to average current-meter measurements over the bottom 500 meters because these values are close to the vertical resolution in the deepest layers of the models, where the current speed comparison takes place. There is a trade-off between the decreasing number of observations available as we get closer to the seafloor and the representativeness of the current speeds farther from the seafloor. An upper boundary at 500 meters above the seafloor allows us to resolve an entire model layer, as well as having a reasonably large number of current-meter observations. Using only data at locations where at least 2 instruments were available within the bottom 500 meters, with seafloor depths exceeding 1000 meters, our current-meter dataset comprises measured current speeds over 378 locations.

3. Results

3.1. Modeled changes in bottom-water properties under the RCP8.5 scenario

According to the CMIP5 model mean temperature predictions throughout this century, an important warming of bottom waters occurs near the continents, where the seafloor is shallow, and in the Southern Ocean (Fig. 1a). Conversely, the bottom-water temperatures in the northwestern Atlantic display a sharp cooling of ~ 0.6 °C by the end of this century, in agreement with the current abyssal cooling trend in this basin [*Desbruyères et al*., 2016]. This is likely attributable to the decline in the meridional overturning circulation strength because the overturning cell becomes shallower and less heat is transported from the surface to the abyss [*Caesar et al*., 2018; *Rhein et al.*, 2011; *Thornalley et al*., 2018; *Zhang*, 2008]. Globally, under the RCP8.5 scenario, mean bottom-water temperatures are projected to increase by ~ 0.2 °C between the first and the last 30 years of this century. Concomitantly, an important freshening of bottom waters is projected in high boreal latitudes, while bottom-waters in the Southern Ocean become saltier (Fig. 1b), in line with the results of *Heuzé et al*. [2015] and *Meijers* [2014]. In contrast, recent studies have reported freshening of Antarctic Bottom Waters (AABW), based on hydrographic data, that is thought to be caused by glacial melting [*Menezes et al*., 2017; *Purkey and Johnson*, 2013]. Warmer and saltier AABW would be consistent with reduced ventilation in this area [*de Lavergne et al*., 2014], as predicted by ESM2M (Fig. S2), as weakening deep convection around Antarctica brings less, relatively cold and fresh waters to the bottom. Coarse

resolution climate models, such as the CMIP5 models used here, generally form AABW by open-ocean convection, something that is thought to rarely happen in nature. Only very fine resolution (greater than 0.1°) models are able to form some AABW from dense water generated on the shelf cascading to the abyss [e.g. *Bryan et al.*, 2014; *Dufour et al.*, 2017; *Newsom et al.*, 2016].

Global bottom-water *DIC* rises by an average of 9 µmol kg^{-1}, i.e., a 0.4% increase relative to the beginning of the century (Fig. 1c). Some of the largest bottom-water *DIC* increases are projected to occur in the northern Atlantic where the bottom waters are youngest [*Huiskamp and Meissner*, 2012; *Matsumoto*, 2007] and rich in anthropogenic CO_2. In the Labrador Sea and at the southern edge of Greenland, the *DIC* increases are as high as +70 µmol kg^{-1}, i.e., a ~3% increase relative to the beginning of the century. We also note an acute increase (+ ~40 µmol kg^{-1}) of *DIC* along the western fringe of the Atlantic and Pacific Oceans. A weaker but more spatially extended *DIC* increase of ~10 µmol kg^{-1} in the southern half of the globe is also predicted, that can be attributed partly to the northward spreading of the dense and young Antarctic Bottom Waters [*de Lavergne et al*., 2017; *Gebbie and Huybers*, 2012]. The elongated positive *DIC* anomaly in the low latitudes of the Pacific Ocean (i.e., between Peru and Melanesia) is driven by an accumulation of metabolic CO_2, as an increase in both the age of bottom waters (see Fig. S2) and the particulate organic carbon sinking flux (see Fig. S3) is predicted in this area. Older bottom waters may reflect weakened bottom currents (see section 4.2) and/or reduced bottom-water mixing. Older bottom waters accumulate more metabolic products (nutrients, *DIC*) resulting from the oxic catabolism of sinking organic material, explaining the positive anomaly in *DIC*, [*SRP*] and [*dSi*] in the equatorial Pacific, Southern Ocean and Northern Atlantic.

Under the RCP8.5 scenario, the global mean bottom-water *TA* is stable, increasing by only ~0.5 µmol kg^{-1} during the 21st century (Fig. 1d). Potential sources for *TA* include $CaCO_3$ dissolution and the addition of nutrients (*SRP* or *dSi*) to seawater. In fact, bottom-water *SRP* (Fig. 1e) and *dSi* (Fig. 1f) concentrations strongly increase in the Atlantic Ocean, while they decrease in the Arctic Ocean, as seen in Fig. 1e-f, and the relative changes in *TA*, *SRP* and *dSi* are highly correlated in most of the bottom waters, as shown in Fig. S4.

The modelled changes in *U* are spatially highly heterogeneous (Fig. 1g) making it challenging to identify coherent regional modifications. Nevertheless, in a warm, high-CO_2 world, the CMIP5 model mean *U* globally declines by ~2% (between 1 and 3 %, depending on the model) by the end of the century. Bottom currents weaken notably near the Equator and Northern Atlantic, and by up to 40% by the end of the century off-shore of Newfoundland.

Finally, the downward flux of calcite reaching the seafloor, *F*, is predicted to show an ubiquitous decline (Fig. 1h). The CMIP5 model mean *F* decreases by 25% (between 11 and 48 %, depending on the model) by the end of the 21st century. We attribute this abated *F* to reduced surface production and export, and increased water-column $CaCO_3$ dissolution. Although the magnitude of *F* decline is greater at low latitudes where the $CaCO_3$ rain rate is highest, the relative *F* decline is greater and more important at high latitudes.

By the end of this century (i.e., average 2071-2100) and outside of the high latitudes, the CMIP5 model mean *CSD* will be 2041 m, which is 146 m shallower than the 2006-2035 average value. In comparison, Sulpis et al. (2018) computed a *CSD* rise of 142 m between the end of the

preindustrial period (i.e., 1800) and 2002. These results suggest that the *CSD* rise is accelerating as we go further into the Anthropocene.

3.2. Calcite dissolution rate

At the end of the 21st century, the fastest benthic $CaCO_3$ dissolution (*r*) will occur in the equatorial Pacific (Fig. 2a), where bottom waters are strongly undersaturated with respect to calcite, sediments are rich in $CaCO_3$ and bottom currents are fast (see Fig. S1). Areas located between the preindustrial and the rising *CCD*, i.e., which corresponds to topographic highs, are associated with important dissolution rate increases, while the deeper areas of the ocean, located below the preindustrial *CCD*, show a dissolution rate decrease. In the eastern equatorial Pacific, meridional shifts in bottom currents will cause abrupt changes in the benthic dissolution rates. In the northern half of the central Pacific, between the Fiji Plateau and the Aleutian Trench, a large area of reduced *r* will develop, explained primarily by a drop in *F* (Fig. 3b). In this area, except for the Hawaiian archipelago, the seafloor is located below the *CCD*. Thus, the calcite dissolution rate at the seafloor is constrained by the calcite rain rate, according to Eq. (5), regardless of any DBL limitation and, thus, independent of bottom currents. The same is true for the southern extents of the Atlantic, Pacific and Indian Oceans, where most of the seafloor is below the *CCD*, and seafloor dissolution depends only on rain rate changes. Although a large amount of anthropogenic CO_2 enters the deep ocean in the North Atlantic, this CO_2 does not spread into the deepest layers of the abyssal Atlantic (see Fig. 1). In fact, most of the seafloor in this basin is covered by colder and denser AABW [*Johnson*, 2008; *Morozov et al*., 2010], nearly devoid of anthropogenic CO_2 except for its most southern extent [*Ríos et al.*, 2015]. As it takes several centuries for the AABW to reach the Equator in the Atlantic Ocean basin [*Huiskamp and Meissner*, 2012].

By isolating the effect of each controlling variable on the overall benthic dissolution rate (Fig. 3a), we reveal that while increasing bottom-water *DIC* globally drives the dissolution rate up during the 21st century, bottom-water total alkalinity (*TA*), bottom-current speeds (*U*) and calcite rain rates (*F*) lower the dissolution rate. A reduction in the calcite flux reaching the deep-ocean (*F*) leads to a lower dissolution rate below the *CCD*, according to Eqs. (5) and (6), and causes the *CCD* to rise much faster [*Boudreau et al*., 2010b]. We estimate that the CMIP5 model mean world-averaged *CCD* will rise from 4465 ± 378 m at the beginning of the 21st century to 3677 ± 715 m by the end of the century - a 788 ± 809 m shoaling in less than a century. Whereas 83 to 168 $x10^6$ km^2 (28 to 57 %) of the seafloor are located below the *CCD* at the beginning of the century (outside of high latitudes), this area grows to between 130 and 243 $x10^6$ km^2 (45 to 83 %) by the end of the century. In other words, due to the predicted *CCD* rise, 61 ± 70 $x10^6$ km^2 (21 ± 24 %) of the seafloor could switch from being the locus of net $CaCO_3$ accumulation to net dissolution. Changes in *F* dominate the 21st century benthic dissolution rate variations over most of the high latitudes and deep abyssal plains, as the seafloor in these areas resides, for the most part, below the *CCD*. *DIC*- and *TA*-driven dissolution rate changes are more important in shallower areas, corresponding to topographic highs or coastal areas, as shown in Fig. 3b. Finally, the global decrease in bottom-current speeds increases the average DBL thickness and leads to a small but widespread slowdown of the calcite dissolution rate at the seafloor. Dissolution rate reduction due to bottom-current changes is important at low latitudes, and over the mid-ocean Indian and Pacific ridges (Fig. 3b). Globally, throughout the 21st century

and under RCP8.5, the calcite rain rate (F) and bottom-current speed (U) govern the seafloor calcite dissolution rate changes over 53% and 31% of the dissolving seafloor (i.e., the area of the seafloor overlain by undersaturated bottom waters), respectively. Other factors, such as *DIC* and *TA*, dominate the calcite dissolution changes over much smaller portions of the seafloor (13% and 3%, respectively). Variations of bottom-water T, S_P, [*SRP*] and [*dSi*] do not exert a strong influence on the benthic dissolution rate, as each impact the rate by less than 1% throughout the 21st century.

4. Discussion

4.1. Formulating calcite dissolution in sediments

The novelty of the current approach rests with the inclusion of the effects of both bottom-water chemistry and current velocity information on dissolution rates. Doing so, we are able to identify areas of focused dissolution where high bottom-water velocities are prevalent as well as areas where climate warming reduces such velocities and associated dissolution. Nevertheless, our dissolution rate model does not include oxic or anoxic respiration-driven dissolution. In Fig. 4, we provide a comparison of our 2006-2035 dissolution rates with those obtained by *Dunne et al*. [2012]. The model developed by *Dunne et al*. [2012] accounts for organic matter respiration within the oxic zone of the sediments, and metabolic CO_2 production, which can locally reduce the porewater calcite saturation state and trigger dissolution regardless of the overlying water column chemistry [*Archer*, 1996; *Mekik et al*., 2002; *Hales*, 2003]. As our computations do not consider metabolic dissolution, our model underestimates dissolution rates relative to those derived by *Dunne et al*. [2012] in areas of high organic carbon fluxes at the seafloor (Fig. 5d). In these areas, future changes in organic carbon fluxes to the seafloor (e.g., see Fig. S3) could affect calcite dissolution in sediments.

Likewise, other factors such as changes in bottom-water temperatures or dissolved oxygen concentrations could influence the activity of burrowing organisms, enhancing or impeding bioirrigation or bioturbation, processes that can locally modify porewater solute distributions and fluxes across the sediment-water interface [*Boudreau and Jørgensen*, 2001; *Meysman et al*., 2006; *Teal et al*., 2008]. Regrettably, in the absence of observations of changes in deep-sea burrowing organism activity and/or in benthic organic carbon fluxes, we cannot expand on this further.

On the other hand, the model of *Dunne et al*. [2012] does not take into consideration the presence of a current-speed dependent DBL above the sediment-water interface. Most sediment models published to date either ignore the presence of a DBL above the sediment-water interface or consider a DBL with a thickness set to a constant arbitrary value [*Boudreau*, 1996; *van Cappellen and Wang*, 1996; *Heinze et al*., 1999; *Archer et al*., 2002; *Hales*, 2003; *Munhoven*, 2007; *Tschumi et al*., 2011]. Instead, the DBL thickness should be expressed as a function of current-speed, as formulated by various authors [*Boudreau and Guinasso*, 1982; *Levich*, 1962; *Higashino and Stefan*, 2004; *Sulpis et al*., 2018] and confirmed by experimentalists [*Larkum et al*., 2003; *Lorke et al*., 2003; *Santschi et al*., 1983; *Santschi et al*., 1991]. As shown in Fig. 4, the present study, which uses a current-speed dependent DBL thickness, predicts dissolution rates that are higher than those derived by *Dunne et al.* [2012] in areas of fast bottom currents. Future

research efforts should focus on developing sediment modules inclusive of both sedimentary organic carbon degradation and mass transfer through a DBL of variable thickness.

According to our calculations, 25.3 ± 16.0 Tmol of $CaCO_3$ dissolve each year at the sediment-water interface at the beginning of the 21st century. In contrast, using the data of *Dunne et al*. [2012], we estimate that only 13 Tmol of $CaCO_3$ are dissolved each year within marine sediments. These values represent only 20.7 and 10.6 %, respectively, of the total pelagic $CaCO_3$ dissolution estimated by *Smith and Mackenzie* [2016]. In comparison, *Berelson et al*. [2007] and *Sulpis et al*. [2018] estimated the modern seafloor calcite dissolution flux at 33 ± 25 and 32 ± 12 Tmol a^{-1}, respectively. The low dissolution rates that we find compared to observational estimates could result from an overestimate of the DBL thickness. Based on CMIP5 bottom-current speeds, to which tidal current speeds were added (see Methods), the CMIP5 model mean DBL thickness is estimated at ~1.8 mm. According to observations, this value can be reached in the deep-sea, but may be too thick for a global mean value, generally thought to be thinner, from 200 μm- to 1 mm-thick [*Santschi et al*., 1991; *Boudreau and Jørgensen*, 2001; *Sulpis et al*., 2018]. The overestimated DBL thickness in models likely results from an underestimate of the bottom-current speeds simulated by models (e.g., velocities arising from mesoscale and submesoscale processes). Overestimating the DBL thickness in a model where the dissolution is limited by diffusion through the DBL, such as ours, underestimates the true dissolution rate, and may explain the discrepancy in the global $CaCO_3$ dissolution magnitude identified above. In the following discussion, we investigate the bottom-current representation in models.

4.2. Modelled bottom currents

Under increasing atmospheric pCO_2, all models tested here predict a bottom-current speed decrease (Fig. 5), and these decreasing trends are statistically significant (Fig. 5 and Table S2). On average, the six models predicted the world-averaged, resolved current speed to drop by 6.8 ± 3.9 % upon doubling of the preindustrial atmospheric pCO_2. As shown in Fig. 5b, all models predict a bottom-current slowdown in several areas of the North Atlantic, the Equatorial Atlantic and most of the Pacific Ocean, consistent with the results of *Cheng et al*. [2013]. This slowdown is likely linked to a weakening of the Atlantic meridional overturning circulation (AMOC) and a reduced ventilation in the North Atlantic [*Caesar et al*., 2018; *Pérez et al*., 2013; *Steinfeldt et al*., 2009; *Thornalley et al*., 2018; *Wanninkhof et al*., 2010; *Zhang*, 2008]. *Collins et al*. [2013] estimated that the strength of the AMOC will drop by 12-54% during the 21st century under RCP8.5. Likewise, in the Southern Ocean, anthropogenic surface-water freshening may cause a weakening in the production of AABW [*de Lavergne et al*., 2014].

Although the trend of decreasing bottom-current over this century is a consistent feature across CMIP5 and CM2-O models, a comparison of these modelled bottom velocities with current-meter observations shows that below 1 km-depth, where most calcite dissolution occurs, these models consistently underestimate bottom-current speeds (Fig. 6). Because neither the models used in this study, nor our current-meter dataset include tides, these discrepancies are due to a lack of resolved motions and physics, not to a lack of tidal velocities in models. Only the HYCOM simulations successfully reproduce the magnitude of observed bottom-current speeds (Fig. 6). Nevertheless, the correlation coefficient of the modelled, resolved current speeds to the

measurements for the HYCOM simulations are lower than those for the CMIP5 and CM2-O models (Fig. 7). The correlations between output of the higher resolution models and the current meter observations are not expected to be as strong as those of the coarser resolution models because of the difficulty of co-locating currents at high resolution. In fact, the correlation coefficients between the outputs of higher resolution models and the current meter observations increase when the higher resolution model outputs are smoothed onto the same grid as the coarser resolution models.

Mesoscale eddies carry a large proportion of the flow from the surface to the bottom and are only resolved for ocean models with horizontal resolutions higher than about $1/5^{th}$ degree at ~30 °N or S, $1/10^{th}$ degree at ~60 °N or S [*Hecht and Hasumi*, 2008; *Hallberg*, 2013]. Thus, the three CMIP5 models used in this study have a horizontal resolution that is too coarse to explicitly resolve these eddies. Instead, these models rely on a mesoscale eddy transport parameterization (see *Gent and McWilliams* [1990]; *Griffies* [1998]). In addition, the use of geopotential-height vertical coordinates requires additional schemes to accurately represent bottom-following flows (e.g., *Adcroft et al.* [1997]) and can result in their misrepresentation [*Dunne et al*., 2012]. In Fig. S5, we show that, in CM2-1deg, the parameterized bottom-current speeds associated with the mesoscale are generally less than 5% of the resolved current speeds, except at high latitudes. Similarly, using the *Marshall and Adcroft* [2010] mesoscale eddy kinetic energy framework, *Melet et al.* [2015] showed that the resolved bottom velocities are generally higher than the parameterized bottom mesoscale velocities. According to *Melet et al*. [2015], the contribution of the parameterized bottom speed to the total bottom speed is of generally 1/3 (Angélique Melet, personal communication) although it is larger in the Southern Ocean; see Fig. 3 in *Melet et al*. [2015]. Thus, it is unlikely that the unresolved, parameterized flows account for the order of magnitude discrepancy between the coarse resolution models and the current-speed observations. *Pearson et al*. [2017] found that reduced water viscosity in models leads to stronger bottom currents. The bottom-current speed underestimation by CM2.6 is surprising, given its relatively high resolution, and we speculate, based upon the *Pearson et al*. [2017] results, that the differences between CM2.6 and the HYCOM simulations might be due to different viscosity coefficients (see e.g., *Griffies and Hallberg* [2000] and *Wallcraft et al*. [2005]), or methods of applying bottom-drag. We also note that, as model resolution is refined in the CM2-O suite, the globally-averaged bottom currents are faster (Fig. 6b). Finally, in regions of rough topography and strong bottom currents, sub-mesoscale instabilities might generate currents with velocities that exceed those resolved by models [e.g., *Callies*, 2018], which could explain some of the discrepancies highlighted here.

In brief, our results of 21^{st}-century dissolution changes being dominated by $CaCO_3$ sinking flux variations rely on several assumptions regarding future bottom currents, all of which could be verified by future research: first, tidal velocities will not be impacted by climate change; second, barotropic tidal velocities dominate over baroclinic tidal velocities near the seafloor; third, CMIP5 models accurately predict the trend in the resolved velocities near the seafloor; fourth, the trend in the (sub)-mesoscale velocities near the seafloor is dominated by the trend in resolved velocities. Notwithstanding, given that mesoscale velocities near the seafloor are also projected to decrease through the 21^{st} century due to anthropogenic CO_2 emissions [*Melet et al*., 2015], the overall bottom speeds - and associated dissolution rate - decrease could be larger than what is reported here.

4.3. Global $CaCO_3$ dissolution and sources of uncertainty

Our results show that $CaCO_3$ dissolution at the seafloor will be delayed by the combination of an abated biogenic $CaCO_3$ delivery to the seafloor, bottom-current slowdown and alkalinisation of bottom waters. Nevertheless, model disagreements reveal large uncertainties regarding the role of controlling variables thus preventing the accurate prediction of $CaCO_3$ cycling at the seafloor over the next century. Fig. 8 represents the global 21st century calcite dissolution rate, computed from the CMIP5 model variables using the sum of the TPXO9.1 tidal velocities and the bottom velocities as resolved by the models. The standard deviation was computed using standard error propagation rules following *Sulpis et al*. [2018]. Despite large cumulative errors that hinder accurate future calcite dissolution predictions, a Mann-Kendall trend test reveals that the global seafloor calcite dissolution rate evolves during the 21st century under RCP8.5 with a statistically significant increasing trend ($p = 2 \times 10^{-5}$).

The uncertainty associated with the computed $[CO_3^{2-}]_{SW}$ was derived using the code from *Orr et al*. [2018]. In year 2100, the scaled-up seafloor calcite dissolution rate is 25.6 ± 10.6 Tmol a^{-1}, statistically indistinguishable from the 2006-2035 averaged rate of 25.3 ± 16.0 Tmol a^{-1}, due to the wide error bars. As can be seen in Fig. 1, the modelled values of many bottom-water variables are different depending on the model. From the three CMIP5 models used in this study, the world-averaged intermodel standard deviations for *TA* and *DIC* are 40 and 66 μmol kg^{-1}, respectively, which represents more than 10 times the usual measurement errors [*Millero*, 2007; *Olsen et al*., 2016]. The computed bottom-water CO_3^{2-} concentration is, thus, highly dependent on the model, which inhibits our ability to accurately simulate dissolution rates in the present or future.

Given that the delivery of biogenic $CaCO_3$ to the seafloor is the primary control on benthic $CaCO_3$ dissolution throughout the 21st century, and that the spread in CMIP5 predictions of $CaCO_3$ rain rate is very large, most of the uncertainty in our dissolution rate predictions originates from the $CaCO_3$ rain rate uncertainty. In fact, the standard deviation across models on the world-averaged calcite flux to the bottom is larger than its mean value throughout the entire century. Whether at the surface ocean or at depth, our inability to precisely quantify the $CaCO_3$ rain rate has already been pointed out by *Berelson et al.* [2007]. Similarly, experimental investigations of the response of $CaCO_3$ surface production to elevated CO_2 conditions have reported disparate responses [*Wootton et al.*, 2008; *Pinsonneault et al.*, 2012; *Fukuda et al.*, 2014; *Maugendre et al.*, 2017]. In the next century, while coccolithophores could initially benefit from elevated CO_2 concentrations, global calcification could ultimately be reduced relative to the end of the preindustrial era, under end-of-the-century RCP8.5 atmospheric CO_2 levels [*Krumhardt et al.*, 2019]. Direct suppression of biogenic $CaCO_3$ production under seawater acidification is absent from many models or otherwise often highly parameterized and probably overly deterministic. There are ongoing debates about what actually drives calcification, which consequently should represent a priority for both experimental and modeling work (see *Fassbender et al*. (2016) and references therein). According to results presented here, an accurate representation of the biogenic $CaCO_3$ export and rain rate in Earth System and climate models should be a priority for future model developments. This recommendation is in line with the conclusion reached by *Boudreau et al.* (2018) on the role of a changing carbonate rain/calcification rate in enhancing or reducing $CaCO_3$ preservation over longer time scales. Independent modelling approaches suggest that the calcification rate is a central player in acidification dynamics.

5. Conclusion

Calcite dissolution rates at the seafloor are controlled by a variety of processes that will evolve under projected warming and acidification. Whereas ocean acidification controls the thermodynamic potential of the dissolution reaction, widening the gap between $[CO_3^{2-}]_{SW}$ and $[CO_3^{2-}]_{eq}$, and driving calcite towards dissolution, the dissolution rate at the seafloor also depends on kinetic processes that are independent of solution chemistry, such as the resistance caused by the presence of a diffusive boundary layer above the seafloor, whose thickness is dependent on bottom-current speeds that are also projected to change. Traditionally, the balance of $CaCO_3$ fluxes at the sediment-water interface has been expected to shift towards enhanced dissolution in response to any acidification event [*Archer et al*., 1998; *Boudreau*, 2013; *Broecker and Peng*, 1982; *Eyre et al*., 2018; *Sulpis et al*., 2018]. Our results show that within the 21st century, when various processes affecting the calcite dissolution rate at the seafloor are considered, the dissolution rate increase is lower that what would be predicted when considering bottom-water acidification only, due to a combination of both a decreasing supply of calcite from above and bottom-current velocity. The general slowdown of bottom-currents and declining $CaCO_3$ flux to the seafloor counteract the effect of ocean acidification on the calcite dissolution rate at the seafloor. One should, however, be wary of simply extrapolating such results over longer time scales.

Over more than half of the dissolving seafloor, benthic $CaCO_3$ dissolution rate changes through the 21st century will be primarily driven by declining $CaCO_3$ rain rates. Thus, a better representation of $CaCO_3$ settling fluxes, as well as the $CaCO_3$ production response to elevated CO_2 concentrations, should be a priority for future model developments. Even though most recent models strongly underestimate modern bottom-current speeds relative to field observations, partly due to the low-resolution of the ocean component, all models tested in this study consistently predict a global decrease in the strength of bottom circulation. To accurately represent the magnitude and loci of calcite dissolution at the seafloor, models must better represent bottom-water chemistry, bottom currents, and integrate a diffusive boundary layer module in which the DBL thickness fluctuates according to the hydrodynamics at the seafloor. This work suggests that seafloor calcite dissolution in response to the ongoing acidification event and its associated CO_2 sink may be delayed and has important implications in our understanding of calcite dissolution and preservation and CO_2 neutralization on geological time scales.

Acknowledgments

The authors declare no conflict of interest. We thank Angélique Melet and Richard E. Thomson for fruitful discussions, as well as Lori Sentman, Robbie Toggweiler and two anonymous reviewers for helpful comments and suggestions. We acknowledge the World Climate Research Programme's Working Group on Coupled Modelling, which is responsible for CMIP, and we thank the individual climate modeling groups for producing and making available their model output. The U.S. Department of Energy's Program for Climate Model Diagnosis and Intercomparison provides coordinating support and led development of the For CMIP software infrastructure in partnership with the Global Organization for Earth System Science Portals. We thank the Geophysical Fluid Dynamics Group (GFDL) at Princeton for sharing the model output

of the CM2-O suite. DST and BKA thank their co-authors in *Trossman et al*. [2016] for allowing them access to the HYCOM results used in this paper. Grants of computer time were provided by the Department of Defense (DoD) High Performance Computing Modernization Program and by the National Center for Atmospheric Research (NCAR) Yellowstone university allocations. DST and BKA thank Rob Scott who compiled the original current meter database that we have modified for use in their papers including this one. OS acknowledges the Department of Earth and Planetary Sciences at McGill University and the Natural Sciences and Engineering Research Council of Canada (through Discovery Grants to AM) for financial support during his residency in the graduate program. All CMIP5 model outputs used in this study are available via the ESGF peer-to-peer enterprise system site (https://esgf-node.llnl.gov/search/cmip5/). CaCO3 sediment contents and CCD distributions are available on the NOAA Ocean Carbon Data System website (https://www.nodc.noaa.gov/ocads/oceans/ndp_099/ndp099.html).

References

Adcroft, A., Hill, C. and Marshall, J. (1997) Representation of Topography by Shaved Cells in a Height Coordinate Ocean Model. *Monthly Weather Review*, 125, 2293-2315, https://doi.org/10.1175/1520-0493(1997)125<2293:ROTBSC>2.0.CO;2

Alexander, K., J. Meissner, K., & J. Bralower, T. (2015). Sudden spreading of corrosive bottom water during the Palaeocene–Eocene Thermal Maximum. *Nature Geoscience, 8*(6), 458-461. doi:10.1038/ngeo2430, https://doi.org/10.1038/NGEO2430

Anderson, L.G., Olsson, K., Jones, E.P., Chierici, M. and Fransson, A. (1998) Anthropogenic carbon dioxide in the Arctic Ocean: Inventory and sinks. *Journal of Geophysical Research: Oceans* 103, 27707-27716, https://doi.org/10.1029/98JC02586

Archer, D. (1996) A data-driven model of the global calcite lysocline. *Global Biogeochemical Cycles* 10: 511-526, https://doi.org/10.1029/96GB01521.

Archer, D., Kheshgi, H. and Maier-Reimer, E. (1998) Dynamics of fossil fuel CO_2 neutralization by marine $CaCO_3$. *Global Biogeochemical Cycles* 12, 259-276, https://doi.org/10.1029/98GB00744

Archer, D.E., Morford, J.L. and Emerson, S.R. (2002) A model of suboxic sedimentary diagenesis suitable for automatic tuning and gridded global domains. *Global Biogeochemical Cycles* 16(1), 17-1-17-21, https://doi.org/10.1029/2000GB001288

Archer, D., Eby, M., Brovkin, V., Ridgwell, A., Cao, L., Mikolajewicz, U., Caldeira, K., Matsumoto, K., Munhoven, G., Montenegro, A. and Tokos, K. (2009) Atmospheric Lifetime of Fossil Fuel Carbon Dioxide. *Annual Review of Earth and Planetary Sciences* 37, 117-134, https://doi.org/10.1146/annurev.earth.031208.100206

Bates, N.R., Best, M.H.P., Neely, K., Garley, R., Dickson, A.G. and Johnson, R.J. (2012) Detecting anthropogenic carbon dioxide uptake and ocean acidification in the North Atlantic Ocean. *Biogeosciences* 9, 2509-2522

Bellouin N., O. Boucher, J. Haywood, C. Johnson, A. Jones, J. Rae, and S. Woodward. (2007) *Improved representation of aerosols for HadGEM2*. Meteorological Office Hadley Centre, Technical Note 73, March 2007

Berelson, W.M., Balch, W.M., Najjar, R., Feely, R.A., Sabine, C. and Lee, K. (2007) Relating estimates of $CaCO_3$ production, export, and dissolution in the water column to measurements of $CaCO_3$ rain into sediment traps and dissolution on the sea floor: A revised global carbonate budget. *Global Biogeochemical Cycles* 21

Boudreau, B.P. (1996) A method-of-lines code for carbon and nutrient diagenesis in aquatic sediments. *Computers & Geosciences* 22(5), 479-496, https://doi.org/10.1016/0098-3004(95)00115-8

Boudreau, B.P. (2013) Carbonate dissolution rates at the deep ocean floor. *Geophysical Research Letters* 40, 744-748, https://doi.org/10.1029/2012GL054231

Boudreau, B.P. and Guinasso, N.L., Jr. (1982) The influence of a diffusive boundary layer on accretion, dissolution, and diagenesis at the sea floor, in: Fanning, K.A., Manheim, F.T. (Eds.), *The Dynamic Environment of the Ocean Floor*. Lexington Books, Lexington, pp. 115-145.

Boudreau, B.P. and Jørgensen, B.B. (2001) *The Benthic Boundary Layer: Transport Processes and Biogeochemistry*. Oxford University Press, Oxford.

Boudreau, B.P. and Luo, Y. (2017) Retrodiction of secular variations in deep-sea CaCO 3 burial during the Cenozoic. *Earth and Planetary Science Letters* 474, 1-12, https://doi.org/10.1016/j.epsl.2017.06.005

Boudreau, B.P., Middelburg, J.J., Hofmann, A.F. and Meysman, F.J.R. (2010a) Ongoing transients in carbonate compensation. *Global Biogeochemical Cycles* 24, https://doi.org/10.1029/2009GB003654

Boudreau, B.P., Middelburg, J.J. and Meysman, F.J.R. (2010b) Carbonate compensation dynamics. *Geophysical Research Letters* 37, https://doi.org/10.1029/2009GL041847

Boudreau, B.P., Middelburg, J.J. and Luo, Y. (2018) The role of calcification in carbonate compensation. *Nature Geoscience* 11, 894-900.

Bramlette, M.N. (1961) Pelagic sediments, in: Sears, M. (Ed.), Oceanography. *Publications of the American Association for the Advancement of Science*, 67, pp. 345-366.

Broecker, W.S. and Peng, T.H. (1982) *Tracers in the Sea*. Lamont-Doherty Geological Observatory, Columbia University, Palisades, New York.

Bryan, F.O., Gent, P.R. and Thomas, R. (2014) Can Southern Ocean Eddy Effects Be Parameterized in Climate Models? *Journal of Climate* 27, 411-425, https://doi.org/10.1175/JCLI-D-12-00759.1

Caesar, L., Rahmstorf, S., Robinson, A., Feulner, G. and Saba, V. (2018) Observed fingerprint of a weakening Atlantic Ocean overturning circulation. *Nature* 556, 191-196, https://doi.org/10.1038/s41586-018-0006-5

Caldeira, K. and Wickett, M.E. (2003) Anthropogenic carbon and ocean pH. *Nature* 425, 365-365, https://doi.org/10.1038/425365a

Callies, J. (2018) Restratification of Abyssal Mixing Layers by Submesoscale Baroclinic Eddies. *Journal of Physical Oceanography* 48, 1995-2010, https://doi.org/10.1175/JPO-D-18-0082.1

Carter, B.R., Feely, R.A., Mecking, S., Cross, J.N., Macdonald, A.M., Siedlecki, S.A., Talley, L.D., Sabine, C.L., Millero, F.J., Swift, J.H., Dickson, A.G. and Rodgers, K.B. (2017) Two decades of Pacific anthropogenic carbon storage and ocean acidification along GO-SHIP sections P16 and P02. *Global Biogeochemical Cycles*, https://doi.org/10.1002/2016GB005485

Chen, C.-T.A. (1982) On the distribution of anthropogenic CO_2 in the Atlantic and Southern oceans. *Deep Sea Research* 29, 563-580, https://doi.org/10.1016/0198-0149(82)90076-0

Cheng, W., Chiang, J.C.H. and Zhang, D. (2013) Atlantic Meridional Overturning Circulation (AMOC) in CMIP5 Models: RCP and Historical Simulations. *Journal of Climate* 26, 7187-7197, https://doi.org/10.1175/JCLI-D-12-00496.1

Ciais, P., Sabine, C., Bala, G., Bopp, L., Brovkin, V., Canadell, J., Chhabra, A., DeFries, R., Galloway, J., Heimann, M., Jones, C., Le Quéré, C., Myneni, R.B., Piao, S. and Thornton, P. (2013) Carbon and Other Biogeochemical Cycles. In: Stocker, T.F., D. Qin, G.-K. Plattner, M. Tignor, S.K. Allen, J. Boschung, A. Nauels, Y. Xia, V. Bex and P.M. Midgley [Eds.] Climate Change 2013: The Physical Science Basis. Contribution of Working Group I to the Fifth Assessment Report of the Intergovernmental Panel on Climate Change. Cambridge University Press, Cambridge, United Kingdom and New York, NY, USA.

Collins, M., Knutti, R., Arblaster, J., Dufresne, J.-L., Fichefet, T., Friedlingstein, P., Gao, X., Gutowski, W.J., Johns, T., Krinner, G., Shongwe, M., Tebaldi, C., Weaver, A.J. and Wehner, M. (2013) Long-term Climate Change: Projections, Commitments and Irreversibility, in: Stocker, T.F., Qin, D., Plattner, G.-K., Tignor, M., Allen, S.K., Boschung, J., Nauels, A., Xia, Y., Bex, V., Midgley, P.M. (Eds.), *Climate Change 2013: The Physical Science Basis. Contribution of Working Group I to the Fifth Assessment Report of the Intergovernmental Panel on Climate Change*. Cambridge University Press, Cambridge, United Kingdom and New York, NY, USA, https://doi.org/10.1017/CBO9781107415324.024

Collins, W.J., Bellouin, N., Doutriaux-Boucher, M., Gedney, N., Halloran, P., Hinton, T., Hughes, J., Jones, C.D., Joshi, M., Liddicoat, S., Martin, G., O'Connor, F., Rae, J., Senior, C., Sitch, S., Totterdell, I., Wiltshire, A. and S. Woodward (2011) Development and evaluation of an Earth-System model – HadGEM2. *Geosci. Model Dev.*, 4, 1051-1075, https://doi.org/10.5194/gmd-4-1051-2011

Dade, W.B. (1993) Near-bed turbulence and hydrodynamic control of diffusional mass transfer at the sea floor. *Limnology and Oceanography* 38, 52-69, https://doi.org/10.4319/lo.1993.38.1.0052

de Lavergne, C., Madec, G., Roquet, F., Holmes, R.M. and McDougall, T.J. (2017) Abyssal ocean overturning shaped by seafloor distribution. *Nature* 551, 181-186, https://doi.org/10.1038/nature24472

de Lavergne, C., Palter, J.B., Galbraith, E.D., Bernardello, R. and Marinov, I. (2014) Cessation of deep convection in the open Southern Ocean under anthropogenic climate change. *Nature Climate Change* 4, 278-282, https://doi.org/10.1038/nclimate2132

Delworth, T.L., Rosati, A., Anderson, W., Adcroft, A.J., Balaji, V., Benson, R., Dixon, K., Griffies, S.M., Lee, H.-C., Pacanowski, R.C., Vecchi, G.A., Wittenberg, A.T., Zeng, F. and Zhang, R. (2012) Simulated Climate and Climate Change in the GFDL CM2.5 High-Resolution Coupled Climate Model. *Journal of Climate* 25, 2755-2781, https://doi.org/10.1175/JCLI-D-11-00316.1

Desbruyères, D.G., Purkey, S.G., McDonagh, E.L., Johnson, G.C. and King, B.A. (2016) Deep and abyssal ocean warming from 35 years of repeat hydrography. *Geophysical Research Letters* 43(19): 10,356-10,365, https://doi.org/10.1002/2016GL070413

Dickson, A.G. (1990) Standard potential of the reaction: $AgCl(s)+1/2H_2(g) = Ag(s)+HCl(aq)$, and the standard acidity constant of the ion HSO_4^- in synthetic sea water from 273.15 to 318.15

K. *The Journal of Chemical Thermodynamics* 22, 113-127, https://doi.org/10.1016/0021-9614(90)90074-Z

Dlugokencky, E. and Tans, P. (2018) *Trends in atmospheric carbon dioxide*. National Oceanic and Atmospheric Aministration, Earth System Research Laboratory (NOAA/ESRL).

Dufour, C.O., Morrison, A.K., Griffies, S.M., Frenger, I., Zanowski, H. and Winton, M. (2017). Preconditioning of the Weddell Sea Polynya by the Ocean Mesoscale and Dense Water Overflows. *Journal of Climate* 30(19), 7719-7737.

Dufresne, J.L., Foujols, M.A., Denvil, S., Caubel, A., Marti, O., Aumont, O., Balkanski, Y., Bekki, S., Bellenger, H., Benshila, R., Bony, S., Bopp, L., Braconnot, P., Brockmann, P., Cadule, P., Cheruy, F., Codron, F., Cozic, A., Cugnet, D., de Noblet, N., Duvel, J.P., Ethé, C., Fairhead, L., Fichefet, T., Flavoni, S., Friedlingstein, P., Grandpeix, J.Y., Guez, L., Guilyardi, E., Hauglustaine, D., Hourdin, F., Idelkadi, A., Ghattas, J., Joussaume, S., Kageyama, M., Krinner, G., Labetoulle, S., Lahellec, A., Lefebvre, M.P., Lefevre, F., Levy, C., Li, Z.X., Lloyd, J., Lott, F., Madec, G., Mancip, M., Marchand, M., Masson, S., Meurdesoif, Y., Mignot, J., Musat, I., Parouty, S., Polcher, J., Rio, C., Schulz, M., Swingedouw, D., Szopa, S., Talandier, C., Terray, P., Viovy, N. and Vuichard, N. (2013) Climate change projections using the IPSL-CM5 Earth System Model: from CMIP3 to CMIP5. *Climate Dynamics* 40, 2123-2165

Dunne, J.P., Hales, B. and Toggweiler, J.R. (2012) Global calcite cycling constrained by sediment preservation controls. Global Biogeochemical Cycles 26

Dunne, J.P., John, J.G., Adcroft, A.J., Griffies, S.M., Hallberg, R.W., Shevliakova, E., Stouffer, R.J., Cooke, W., Dunne, K.A., Harrison, M.J., Krasting, J.P., Malyshev, S.L., Milly, P.C.D., Phillipps, P.J., Sentman, L.T., Samuels, B.L., Spelman, M.J., Winton, M., Wittenberg, A.T. and Zadeh, N. (2012) GFDL's ESM2 Global Coupled Climate–Carbon Earth System Models. Part I: Physical Formulation and Baseline Simulation Characteristics. *Journal of Climate* 25, 6646-6665, https://doi.org/10.1175/JCLI-D-11-00560.1

Dunne, J.P., John, J.G., Shevliakova, E., Stouffer, R.J., Krasting, J.P., Malyshev, S.L., Milly, P.C.D., Sentman, L.T., Adcroft, A.J., Cooke, W., Dunne, K.A., Griffies, S.M., Hallberg, R.W., Harrison, M.J., Levy, H., Wittenberg, A.T., Phillips, P.J. and Zadeh, N. (2013) GFDL's ESM2 Global Coupled Climate–Carbon Earth System Models. Part II: Carbon System Formulation and Baseline Simulation Characteristics. *Journal of Climate* 26, 2247-2267, https://doi.org/10.1175/JCLI-D-12-00150.1

Dutkiewicz, A., Müller, R.D., O'Callaghan, S. and Jónasson, H. (2015) Census of seafloor sediments in the world's ocean. *Geology* 43, 795-798, https://doi.org/10.1130/G36883.1

Edmond, J.M. (1974) On the dissolution of carbonate and silicate in the deep ocean. *Deep Sea Research* 21, 455-480, https://doi.org/10.1016/0011-7471(74)90094-1

Egbert, G.D. and Erofeeva, S.Y. (2002) Efficient Inverse Modeling of Barotropic Ocean Tides. *Journal of Atmospheric and Oceanic Technology* 19, 183-204, https://doi.org/10.1175/1520-0426(2002)019<0183:EIMOBO>2.0.CO;2

Eyre, B.D., Cyronak, T., Drupp, P., Carlo, E.H.D., Sachs, J.P. and Andersson, A.J. (2018) Coral reefs will transition to net dissolving before end of century. *Science* 359, 908-911, https://doi.org/10.1126/science.aao1118

Fassbender, A.J., Sabine, C.L. and Feifel, K.M. (2016) Consideration of coastal carbonate chemistry in understanding biological calcification. *Geophysical Research Letters* 43(9), 4467-4476.

Feely, R.A., Sabine, C.L., Lee, K., Millero, F.J., Lamb, M.F., Greeley, D., Bullister, J.L., Key, R.M., Peng, T.H., Kozyr, A., Ono, T. and Wong, C.S. (2002) In situ calcium carbonate dissolution in the Pacific Ocean. *Global Biogeochemical Cycles* 16, 91-91-91-12, https://doi.org/10.1029/2002GB001866

Fukuda, S.Y., Suzuki, Y. and Shiraiwa, Y. (2014) Difference in physiological responses of growth, photosynthesis and calcification of the coccolithophore Emiliania huxleyi to acidification by acid and CO_2 enrichment. *Photosynthesis Research* 121, 299-309, https://doi.org/10.1007/s11120-014-9976-9

Garner, S.T. (2005) A Topographic Drag Closure Built on an Analytical Base Flux. *Journal of the Atmospheric Sciences* 62, 2302-2315, https://doi.org/10.1175/JAS3496.1

Gebbie, G. and Huybers, P. (2012) The Mean Age of Ocean Waters Inferred from Radiocarbon Observations: Sensitivity to Surface Sources and Accounting for Mixing Histories. *Journal of Physical Oceanography* 42, 291-305, https://doi.org/10.1175/JPO-D-11-043.1

Gent, P. R. and McWilliams, J. C. (1990) Isopycnal Mixing in Ocean Circulation Models. *Journal of Physical Oceanography* 20, 150-155, https://doi.org/10.1175/1520-0485(1990)020<0150:IMIOCM>2.0.CO;2

Giorgetta, M.A., Jungclaus, J., Reick, C.H., Legutke, S., Bader, J., Böttinger, M., Brovkin, V., Crueger, T., Esch, M., Fieg, K., Glushak, K., Gayler, V., Haak, H., Hollweg, H.-D., Ilyina, T., Kinne, S., Kornblueh, L., Matei, D., Mauritsen, T., Mikolajewicz, U., Mueller, W., Notz, D., Pithan, F., Raddatz, T., Rast, S., Redler, R., Roeckner, E., Schmidt, H., Schnur, R., Segschneider, J., Six, K.D., Stockhause, M., Timmreck, C., Wegner, J., Widmann, H., Wieners, K.-H., Claussen, M., Marotzke, J. and Stevens, B. (2013) Climate and carbon cycle changes from 1850 to 2100 in MPI-ESM simulations for the Coupled Model Intercomparison Project phase 5. *Journal of Advances in Modeling Earth Systems* 5, 572-597, https://doi.org/10.1002/jame.20038

Griffies, S.M. (1998) The Gent–McWilliams Skew Flux. *Journal of Physical Oceanography* 28, 831-841, https://doi.org/10.1175/1520-0485(1998)028<0831:TGMSF>2.0.CO;2

Griffies, S. M. and R. W. Hallberg. (2000) Biharmonic friction with a Smagorinsky-like viscosity for use in large-scale eddy-permitting ocean models. *Monthly Weather Review* 128, 2935-2946.

Griffies, S.M., Winton, M., Anderson, W.G., Benson, R., Delworth, T.L., Dufour, C.O., Dunne, J.P., Goddard, P., Morrison, A.K., Rosati, A., Wittenberg, A.T., Yin, J. and Zhang, R. (2015) Impacts on Ocean Heat from Transient Mesoscale Eddies in a Hierarchy of Climate Models. *Journal of Climate* 28, 952-977, https://doi.org/10.1175/JCLI-D-14-00353.1

Hales, B. (2003) Respiration, dissolution, and the lysocline. *Paleoceanography and Paleoclimatology* 18: https://doi.org/10.1029/2003PA000915.

Hallberg, R. (2013) Using a resolution function to regulate parameterizations of oceanic mesoscale eddy effects. *Ocean Modelling* 72, 92-103.

Hecht and Hasumi (2008) AGU Monograph. Hecht, M. W., and H. Hasumi, Eds., 2008: Ocean Modeling in an Eddying Regime. *Geophys. Monogr*., Vol. 177, Amer. Geophys. Union, 409 pp, https://doi.org/10.1029/GM177

Heinze, C., Maier-Reimer, E., Winguth, A.M.E. and Archer, D. (1999) A global oceanic sediment model for long- term climate studies. *Global Biogeochemical Cycles* 13(1), 221-250, https://doi.org/10.1029/98GB02812

Heuzé, C., Heywood, K.J., Stevens, D.P. and Ridley, J.K. (2015) Changes in Global Ocean Bottom Properties and Volume Transports in CMIP5 Models under Climate Change Scenarios. *Journal of Climate* 28, 2917-2944, https://doi.org/10.1175/JCLI-D-14-00381.1

Higashino, M., and Stefan, H. G. (2004) Diffusive boundary layer development above a sediment-water interface. *Water Environment Research* 76: 292-300, https://doi.org/10.2175/106143004X141870.

Huiskamp, W.N. and Meissner, K.J. (2012) Oceanic carbon and water masses during the Mystery Interval: A model-data comparison study. *Paleoceanography* 27, https://doi.org/10.1029/2012PA002368

Johnson, G.C. (2008) Quantifying Antarctic Bottom Water and North Atlantic Deep Water volumes. *Journal of Geophysical Research* 113, https://doi.org/10.1029/2007JC004477

Joos, F. and Spahni, R. (2008) Rates of change in natural and anthropogenic radiative forcing over the past 20,000 years. *Proceedings of the National Academy of Sciences* 105, 1425-1430, https://doi.org/10.1073/pnas.0707386105

Kendall, M.G. (1975) *Rank Correlation Methods*. Charles Griffin, London, UK.

Khatiwala, S., Primeau, F. and Hall, T. (2009) Reconstruction of the history of anthropogenic CO_2 concentrations in the ocean. *Nature* 462, 346-349, https://doi.org/10.1038/nature08526

Körtzinger, A., Mintrop, L. and Duinker, J.C. (1998) On the penetration of anthropogenic CO_2 into the North Atlantic Ocean. *Journal of Geophysical Research: Oceans* 103, 18681-18689, https://doi.org/10.1029/98JC01737

Krumhardt, K. M., N. S. Lovenduski, M. C. Long, M. Levy, K. Lindsay, J. K. Moore and C. Nissen (2019). Coccolithophore Growth and Calcification in an Acidified Ocean: Insights From Community Earth System Model Simulations. *Journal of Advances in Modeling Earth Systems* 11, 1418-1437, https://doi.org/10.1029/2018MS001483

Larkum, A.W.D., Koch, E.M.W., and Kühl, M. (2003) Diffusive boundary layers and photosynthesis of the epilithic algal community of coral reefs. *Marine Biology* 142: 1073-1082, https://doi.org/10.1007/s00227-003-1022-y.

Lauvset, S.K., Key, R.M., Olsen, A., Heuven, S.v., Velo, A., Lin, X., Schirnick, C., Kozyr, A., Tanhua, T., Hoppema, M., Jutterström, S., Steinfeldt, R., Jeansson, E., Ishii, M., Perez, F.F., Suzuki, T. and Watelet, S. (2016) A new global interior ocean mapped climatology: the 1° × 1° GLODAP version 2. *Earth System Science Data* 8, 325-340, https://doi.org/10.5194/essd-8-325-2016

Le Quéré, C., Andrew, R.M., Friedlingstein, P., Sitch, S., Pongratz, J., Manning, A.C., Korsbakken, J.I., Peters, G.P., Canadell, J.G., Jackson, R.B., Boden, T.A., Tans, P.P., Andrews, O.D., Arora, V.K., Bakker, D.C.E., Barbero, L., Becker, M., Betts, R.A., Bopp, L., Chevallier, F., Chini, L.P., Ciais, P., Cosca, C.E., Cross, J., Currie, K., Gasser, T., Harris, I., Hauck, J., Haverd, V., Houghton, R.A., Hunt, C.W., Hurtt, G., Ilyina, T., Jain, A.K., Kato, E., Kautz, M., Keeling, R.F., Klein Goldewijk, K., Körtzinger, A., Landschützer, P., Lefèvre, N., Lenton, A., Lienert, S., Lima, I., Lombardozzi, D., Metzl, N., Millero, F., Monteiro, P.M.S., Munro, D.R., Nabel, J.E.M.S., Nakaoka, S.-i., Nojiri, Y., Padin, X.A., Peregon, A., Pfeil, B., Pierrot, D.,

Poulter, B., Rehder, G., Reimer, J., Rödenbeck, C., Schwinger, J., Séférian, R., Skjelvan, I., Stocker, B.D., Tian, H., Tilbrook, B., Tubiello, F.N., van der Laan-Luijkx, I.T., van der Werf, G.R., van Heuven, S., Viovy, N., Vuichard, N., Walker, A.P., Watson, A.J., Wiltshire, A.J., Zaehle, S. and Zhu, D. (2018) Global Carbon Budget 2017. *Earth System Science Data* 10, 405-448, https://doi.org/10.5194/essd-10-405-2018

Levich, V. G. (1962) *Physicochemical Hydrodynamics*, Prentice-Hall.

Lorke, A., Müller, B., Maerki, M., and Wüest, A. (2003) Breathing sediments: The control of diffusive transport across the 530 sediment-water interface by periodic boundary- layer turbulence. *Limnology and Oceanography* 48: 2077-2085, https://doi.org/10.4319/lo.2003.48.6.2077.

Luecke, C.A., Arbic, B.K., Bassette, S.L., Richman, J.G., Shriver, J.F., Alford, M.H., Smedstad, O.M., Timko, P.G., Trossman, D.S. and Wallcraft, A.J. (2017) The Global Mesoscale Eddy Available Potential Energy Field in Models and Observations. *Journal of Geophysical Research: Oceans* 122, 9126-9143, https://doi.org/10.1002/2017JC013136

Lueker, T.J., Dickson, A.G. and Keeling, C.D. (2000) Ocean pCO_2 calculated from dissolved inorganic carbon, alkalinity, and equations for K_1 and K_2: validation based on laboratory measurements of CO_2 in gas and seawater at equilibrium. *Marine Chemistry* 70, 105-119, https://doi.org/10.1016/S0304-4203(00)00022-0

MacGilchrist, G.A., Garabato, A.C.N., Brown, P.J., Jullion, L., Bacon, S., Bakker, D.C.E., Hoppema, M., Meredith, M.P. Torres-Valdés, S. (2019). Reframing the carbon cycle of the subpolar Southern Ocean. *Science Advances* 5: eaav6410.

Mackenzie, F. and Andersson, A. (2013) The Marine Carbon System and Ocean Acidification during Phanerozoic Time. *Geochemical Perspectives*, 1-227, https://doi.org/10.7185/geochempersp.2.1

Mann, H.B. (1945) Nonparametric tests against trend. *Econometrica* 13, 245-259.

Marshall, D.P. and Adcroft, A.J. (2010) Parameterization of ocean eddies: Potential vorticity mixing, energetics and Arnold's first stability theorem. *Ocean Modelling* 32, 188-204, https://doi.org/10.1016/j.ocemod.2010.02.001

Matsumoto, K. (2007) Radiocarbon-based circulation age of the world oceans. *Journal of Geophysical Research* 112, https://doi.org/10.1029/2007JC004095

Maugendre, L., Gattuso, J.-P., Poulton, A.J., Dellisanti, W., Gaubert, M., Guieu, C. and Gazeau, F. (2017) No detectable effect of ocean acidification on plankton metabolism in the NW oligotrophic Mediterranean Sea: results from two mesocosm studies. *Estuarine, Coastal and Shelf Science* 186(A), 89-99, https://doi.org/10.1016/j.ecss.2015.03.009

McDougall, T.J. and Barker, P.M. (2011) *Getting started with TEOS-10 and the Gibbs Seawater (GSW) Oceanographic Toolbox*. SCOR/IAPSO WG127, p. 28.

McNeil, B.I., Matear, R.J., Key, R.M., Bullister, J.L. and Sarmiento, J.L. (2003) Anthropogenic CO_2 Uptake by the Ocean Based on the Global Chlorofluorocarbon Data Set. *Science* 299, 235-239, https://doi.org/10.1126/science.1077429

Meijers, A.J.S. (2014) The Southern Ocean in the Coupled Model Intercomparison Project phase 5. *Philosophical Transactions of the Royal Society A* 372, 20130296, https://doi.org/10.1098/rsta.2013.0296

Meinshausen, M., Smith, S.J., Calvin, K., Daniel, J.S., Kainuma, M.L.T., Lamarque, J.F., Matsumoto, K., Montzka, S.A., Raper, S.C.B., Riahi, K., Thomson, A., Velders, G.J.M. and van Vuuren, D.P.P. (2011) The RCP greenhouse gas concentrations and their extensions from 1765 to 2300. *Climatic Change* 109, 213-241, https://doi.org/10.1007/s10584-011-0156-z

Mekik F. A., P. W. Loubere, and D. E. Archer, Organic carbon flux and organic carbon to calcite flux ratio recorded in deep-sea carbonates: Demonstration and a new proxy. *Global Biogeochemical Cycles* 16, https://doi.org/10.1029/2001GB001634.

Melet, A., Hallberg, R., Adcroft, A., Nikurashin, M. and Legg, S. (2015) Energy flux into internal Lee waves: sensitivity to future climate changes using linear theory and a climate model. *Journal of Climate* 28, 2365-2384, https://doi.org/10.1175/JCLI-D-14-00432.1

Menezes, V.V., Macdonald, A.M. and Schatzman, C. (2017) Accelerated freshening of Antarctic Bottom Water over the last decade in the Southern Indian Ocean. *Science Advances* 3, https://doi.org/10.1126/sciadv.1601426

Meysman, F.J.R., Galaktionov, O.S., Gribsholt, B. and Middelburg, J.J. (2006) Bioirrigation in permeable sediments: Advective pore- water transport induced by burrow ventilation. *Limnology and Oceanography* 51: 142-156, https://doi.org/10.4319/lo.2006.51.1.0142.

Millero, F.J. (1995) Thermodynamics of the carbon dioxide system in the oceans. *Geochimica et Cosmochimica Acta* 59, 661-677, https://doi.org/10.1016/0016-7037(94)00354-O

Millero, F.J. (2007) The Marine Inorganic Carbon Cycle. *Chemical Reviews*, 107: 308-341, https://doi.org/10.1021/cr05557.

Morozov, E.G., Demidov, A.N., Tarakanov, R.Y. and Zenk, W. (2010) *Deep Water Masses of the South and North Atlantic, Abyssal Channels in the Atlantic Ocean*. Springer, Dordrecht. https://doi.org/10.1007/978-90-481-9358-5_2

Morse, J.W. and Arvidson, R.S. (2002) The dissolution kinetics of major sedimentary carbonate minerals. *Earth-Science Reviews* 58, 51-84, https://doi.org/10.1016/S0012-8252(01)00083-6

Morse, J.W., Arvidson, R.S. and Lüttge, A. (2007) Calcium Carbonate Formation and Dissolution. *Chemical Reviews* 107, 342-381, https://doi.org/10.1021/cr050358j

Morse, J.W. and Mackenzie, F.T. (1990) *Geochemistry of Sedimentary Carbonates*. Elsevier, Amsterdam.

Mucci, A. (1983) The solubility of calcite and aragonite in seawater at various salinities, temperatures and one atmosphere total pressure. *American Journal of Science* 283, 780-799, http://doi.org/10.2475/ajs.283.7.780

Munhoven, G. (2007) Glacial–interglacial rain ratio changes: Implications for atmospheric CO_2 and ocean–sediment interaction. *Deep Sea Research Part II: Topical Studies in Oceanography* 54(5-7), 722-746, https://doi.org/10.1016/j.dsr2.2007.01.008

Naviaux, J.D., Subhas, A.V., Rollins, N.E., Dong, S., Berelson, W.B. and Adkins, J.F. (2019). Temperature dependence of calcite dissolution kinetics in seawater. *Geochimica et Cosmochimica Acta* 246: 363-384, https://doi.org/10.1016/j.gca.2018.11.037

Newsom, E.R., Bitz, C.M., Bryan, F.O., Abernathey, R. and Gent, P.R. (2016) Southern Ocean Deep Circulation and Heat Uptake in a High-Resolution Climate Model. *Journal of Climate* 29, 2597-2619, https://doi.org/10.1175/JCLI-D-15-0513.1

Orr, J.C., Fabry, V.J., Aumont, O., Bopp, L., Doney, S.C., Feely, R.A., Gnanadesikan, A., Gruber, N., Ishida, A., Joos, F., Key, R.M., Lindsay, K., Maier-Reimer, E., Matear, R., Monfray, P., Mouchet, A., Najjar, R.G., Plattner, G.K., Rodgers, K.B., Sabine, C.L., Sarmiento, J.L., Schlitzer, R., Slater, R.D., Totterdell, I.J., Weirig, M.F., Yamanaka, Y. and Yool, A. (2005) Anthropogenic ocean acidification over the twenty-first century and its impact on calcifying organisms. *Nature* 437, 681-686, https://doi.org/10.1038/nature04095

Orr, J.C., Epitalon, J.-M., Dickson, A.G. and Gattuso, J.-P. (2018) Routine uncertainty propagation for the marine carbon dioxide system. *Marine Chemistry* 207: 84-107, https://doi.org/10.1016/j.marchem.2018.10.006

Olsen, A., Key, R. M., van Heuven, S., Lauvset, S. K., Velo, A., Lin, X., Schirnick, C., Kozyr, A., Tanhua, T., Hoppema, M., Jutterström, S., Steinfeldt, R., Jeansson, E., Ishii, M., Pérez, F. F., and Suzuki, T. (2016) The Global Ocean Data Analysis Project version 2 (GLODAPv2) – an internally consistent data product for the world ocean, *Earth System Science Data*, 8, 297-323, https://doi.org/10.5194/essd-8-297-2016.

Pearson, B., Fox-Kemper, B., Bachman, S.D. and Bryan, F.O. (2017) Evaluation of scale-aware subgrid mesoscale eddy models in a global eddy-rich model. *Ocean Modelling* 115: 42–58, https://doi.org/10.1016/j.ocemod.2017.05.007

Perez, F.F., Fontela, M., Garcia-Ibanez, M.I., Mercier, H., Velo, A., Lherminier, P., Zunino, P., de la Paz, M., Alonso-Perez, F., Guallart, E.F. and Padin, X.A. (2018) Meridional overturning circulation conveys fast acidification to the deep Atlantic Ocean. *Nature* 554, 515-518, https://doi.org/10.1038/nature25493

Pérez, F.F., Mercier, H., Vázquez-Rodríguez, M., Lherminier, P., Velo, A., Pardo, P.C., Rosón, G. and Ríos, A.F. (2013) Atlantic Ocean CO_2 uptake reduced by weakening of the meridional overturning circulation. *Nature Geoscience* 6, 146-152,

Pierrot, D., Lewis, E. and Wallace, D. (2006) *MS Excel Program Developed for CO_2 System Calculations*. ORNL/CDIAC-105a, Carbon Dioxide Information Analysis Center, Oak Ridge National Laboratory, U.S. Department of Energy, Oak Ridge, Tennessee.

Pinsonneault, A.J., Matthews, H.D., Galbraith, E.D. and Schmittner, A. (2012) Calcium carbonate production response to future ocean warming and acidification. *Biogeosciences* 9(6), 2351-2364, https://doi.org/10.5194/bg-9-2351-2012

Purkey, S.G. and Johnson, G.C. (2010) Warming of Global Abyssal and Deep Southern Ocean Waters between the 1990s and 2000s: Contributions to Global Heat and Sea Level Rise Budgets. *Journal of Climate* 23, 6336-6351, https://doi.org/10.1175/2010JCLI3682.1

Purkey, S.G. and Johnson, G.C. (2012) Global Contraction of Antarctic Bottom Water between the 1980s and 2000s. *Journal of Climate* 25, 5830-5844 https://doi.org/10.1175/JCLI-D-11-00612.1

Purkey, S.G. and Johnson, G.C. (2013) Antarctic Bottom Water Warming and Freshening: Contributions to Sea Level Rise, Ocean Freshwater Budgets, and Global Heat Gain. *Journal of Climate* 26, 6105-6122, https://doi.org/10.1175/JCLI-D-12-00834.1

Riahi, K., Rao, S., Krey, V., Cho, C., Chirkov, V., Fischer, G., Kindermann, G., Nakicenovic, N. and Rafaj, P. (2011) RCP 8.5-A scenario of comparatively high greenhouse gas emissions. *Climatic Change* 109, 33-57, https://doi.org/10.1007/s10584-011-0149-y

Ridgwell, A. and Hargreaves, J.C. (2007) Regulation of atmospheric CO_2 by deep-sea sediments in an Earth system model. *Global Biogeochemical Cycles* 21, https://doi.org/10.1029/2006GB002764

Riley, J.P. and Tongudai, M. (1967) The major cation/chlorinity ratios in sea water. *Chemical Geology* 2, 263-269, https://doi.org/10.1016/0009-2541(67)90026-5

Ríos, A.F., Resplandy, L., García-Ibáñez, M.I., Fajar, N.M., Velo, A., Padin, X.A., Wanninkhof, R., Steinfeldt, R., Rosón, G. and Pérez, F.F. (2015) Decadal acidification in the water masses of the Atlantic Ocean. *Proceedings of the National Academy of Sciences of the United States of America* 112, 9950-9955, https://doi.org/10.1073/pnas.1504613112

Rhein, M., Kieke, D., Hüttl-Kabus, S., Roessler, A., Mertens, C., Meissner, R., Klein, B., Böning, C.W. and Yashayaev, I. (2011). Deep water formation, the subpolar gyre, and the meridional overturning circulation in the subpolar North Atlantic. *Deep Sea Research Part II: Topical Studies in Oceanography* 58(17-18), 1819-1832.

Sabine, C.L., Feely, R.A., Key, R.M., Bullister, J.L., Millero, F.J., Lee, K., Peng, T.H., Tilbrook, B., Ono, T. and Wong, C.S. (2002) Distribution of anthropogenic CO_2 in the Pacific Ocean. *Global Biogeochemical Cycles* 16, 30-31-30-17, https://doi.org/10.1029/2001GB001639

Santschi, P. H., Bower, P., Nyffeler, U. P., Azevedo, A., and Broecker, W. S. (1983) Estimates of the resistance to chemical transport posed by the deep-sea boundary layer. *Limnology and Oceanography* 28: 899-912, https://doi.org/10.4319/lo.1983.28.5.0899.

Santschi, P.H., Anderson, R.F., Fleisher, M.Q. and Bowles, W. (1991) Measurements of diffusive sublayer thicknesses in the ocean by alabaster dissolution, and their implications for the measurements of benthic fluxes. *Journal of Geophysical Research: Oceans* 96, 10641-10657, https://doi.org/10.1029/91JC00488

Saynisch, J., Petereit, J., Irrgang, C., Kuvshinov, A. and Thomas, M. (2016) Impact of climate variability on the tidal oceanic magnetic signal - A model- based sensitivity study. *Journal of Geophysical Research: Oceans* 121, 5931-5941, https://doi.org/10.1002/2016JC012027

Schlichting, H. (1979) *Boundary Layer Theory*. McGraw-Hill, New York.

Smith, S.V. and Mackenzie, F.T. (2016). The role of $CaCO_3$ reactions in the contemporary CO_2 cycle. *Aquatic Geochemistry* 22(2), 153-175, https://doi.org/10.1007/s10498-015-9282-y

Steinberger, N. and Hondzo, M. (1999) Diffusional Mass Transfer at Sediment-Water Interface. *Journal of Environmental Engineering* 125, 192-200, https://doi.org/10.1061/(ASCE)0733-9372(1999)125:2(192)

Steinfeldt, R., Rhein, M., Bullister, J.L. and Tanhua, T. (2009) Inventory changes in anthropogenic carbon from 1997-2003 in the Atlantic Ocean between 20°S and 65°N. *Global Biogeochemical Cycles* 23, https://doi.org/10.1029/2008GB003311

Sulpis, O., Boudreau, B.P., Mucci, A., Jenkins, C.J., Trossman, D.S., Arbic, B.K. and Key, R.M. (2018) Current $CaCO_3$ dissolution at the seafloor caused by anthropogenic CO_2. *Proceedings of the National Academy of Sciences* 115, 11700-11705, https://doi.org/10.1073/pnas.1804250115

Sulpis, O., Lix, C., Mucci, A. and Boudreau, B.P. (2017) Calcite dissolution kinetics at the sediment-water interface in natural seawater. *Marine Chemistry* 195, 70-83, https://doi.org/10.1016/j.marchem.2017.06.005

Teal, L.R., Bulling, M.T., Parker, E.R. and Solan, M. (2008) Global patterns of bioturbation intensity and mixed depth of marine soft sediments. Aquatic Biology 2: 207-218, https://doi.org/10.3354/ab00052.

Thornalley, D.J.R., Oppo, D.W., Ortega, P., Robson, J.I., Brierley, C.M., Davis, R., Hall, I.R., Moffa-Sanchez, P., Rose, N.L., Spooner, P.T., Yashayaev, I. and Keigwin, L.D. (2018) Anomalously weak Labrador Sea convection and Atlantic overturning during the past 150 years. *Nature* 556, 227-230, https://doi.org/10.1038/s41586-018-0007-4

Timko, P. G., Arbic, B. K., Richman, J. G., Scott, R. B., Metzger, E. J., & Wallcraft, A. J. (2013). Skill testing a three-dimensional global tide model to historical current meter records. *Journal of Geophysical Research: Oceans*, *118*(12), 6914-6933, https://doi.org/10.1002/2013jc009071

Trossman, D.S., Arbic, B.K., Garner, S.T., Goff, J.A., Jayne, S.R., Metzger, E.J. and Wallcraft, A.J. (2013) Impact of parameterized lee wave drag on the energy budget of an eddying global ocean model. *Ocean Modelling* 72, 119-142, http://doi.org/10.1016/j.ocemod.2013.08.006

Trossman, D.S., Arbic, B.K., Richman, J.G., Garner, S.T., Jayne, S.R. and Wallcraft, A.J. (2016) Impact of topographic internal lee wave drag on an eddying global ocean model. *Ocean Modelling* 97, 109-128, https://doi.org/10.1016/j.ocemod.2015.10.013

Tschumi, T., Joos, F., Gehlen, M. and Heinze, C. (2011) Deep ocean ventilation, carbon isotopes, marine sedimentation and the deglacial CO_2 rise. *Climate of the Past* 7(3), 771-800, https://doi.org/10.5194/cp-7-771-2011

van Heuven, S., Pierrot, D., Rae, J.W.B., Lewis, E. and Wallace, D.W.R. (2011) *MATLAB Program Developed for CO2 System Calculations*. ORNL/CDIAC-105b. Carbon Dioxide Information Analysis Center, Oak Ridge National Laboratory, U.S. Department of Energy, Oak Ridge, Tennessee. https://doi.org/10.3334/CDIAC/otg.CO2SYS_MATLAB_v1.1

van Cappellen, P. and Wang, Y. (1996) Cycling of iron and manganese in surface sediments; a general theory for the coupled transport and reaction of carbon, oxygen, nitrogen, sulfur, iron, and manganese. *American Journal of Science* 296(3), 197-243, https://doi.org/10.2475/ajs.296.3.197

van Vuuren, D.P., Edmonds, J., Kainuma, M., Riahi, K., Thomson, A., Hibbard, K., Hurtt, G.C., Kram, T., Krey, V., Lamarque, J.-F., Masui, T., Meinshausen, M., Nakicenovic, N., Smith, S.J. and Rose, S.K. (2011) The representative concentration pathways: an overview. *Climatic Change* 109, 5-31, https://doi.org/10.1007/s10584-011-0148-z

Vázquez-Rodríguez, M., Touratier, F., Monaco, C.L., Waugh, D.W., Padin, X.A., Bellerby, R.G.J., Goyet, C., Metzl, N., Ríos, A.F. and Pérez, F.F. (2009) Anthropogenic carbon distributions in the Atlantic Ocean: data-based estimates from the Arctic to the Antarctic. *Biogeosciences* 6, 439-451, https://doi.org/10.5194/bg-6-439-2009

Voldoire, A., Sanchez-Gomez, E., Mélia, D.S.y., Decharme, B., Cassou, C., Sénési, S., Valcke, S., Beau, I., Alias, A., Chevallier, M., Déqué, M., Deshayes, J., Douville, H., Fernandez, E., Madec, G., Maisonnave, E., Moine, M.-P., Planton, S., Saint-Martin, D., Szopa, S., Tyteca, S., Alkama, R., Belamari, S., Braun, A., Coquart, L. and Chauvin, F. (2013) The CNRM-CM5.1 global climate model: description and basic evaluation. *Climate Dynamics* 40, 2091-2121, https://doi.org/10.1007/s00382-011-1259-y

Wallcraft, A. J., A. B. Kara, and H. E. Hurlburt. (2005) Convergence of Laplacian diffusion versus resolution of an ocean model. *Geophysical Research Letters* 32, L07604, https://doi.org/doi:10.1029/2005GL022514

Wanninkhof, R., Doney, S.C., Bullister, J.L., Levine, N.M., Warner, M. and Gruber, N. (2010) Detecting anthropogenic CO_2 changes in the interior Atlantic Ocean between 1989 and 2005. *Journal of Geophysical Research* 115, https://doi.org/10.1029/2010JC006251

Wanninkhof, R., Park, G.-H., Takahashi, T., Feely, R.A., Bullister, J.L. and Doney, S.C. (2013) Changes in deep-water CO_2 concentrations over the last several decades determined from discrete pCO_2 measurements. *Deep Sea Research Part I* 74, 48-63, https://doi.org/10.7916/D8QJ7T4F

Winton, M., Anderson, W.G., Delworth, T.L., Griffies, S.M., Hurlin, W.J. and Rosati, A. (2014) Has coarse ocean resolution biased simulations of transient climate sensitivity? *Geophysical Research Letters* 41, 8522-8529, https://doi.org/10.1002/2014GL061523

Woosley, R.J., Millero, F.J. and Wanninkhof, R. (2016) Rapid anthropogenic changes in CO_2 and pH in the Atlantic Ocean: 2003-2014. *Global Biogeochemical Cycles* 30, 70-90, https://doi.org/10.1002/2015GB005248

Wootton, J.T., Pfister, C.A., Forester, J.D. (2008) Dynamic patterns and ecological impacts of declining ocean pH in a high-resolution multi-year dataset. *Proceedings of the National Academy of Science of the United States of America* 105(48), 18848-18853, https://doi.org/10.1073/pnas.0810079105

Zeebe, R.E. (2011) On the molecular diffusion coefficients of dissolved CO_2, HCO_3^-, and CO_3^{2-} and their dependence on isotopic mass. *Geochimica et Cosmochimica Acta* 75, 2483-2498, https://doi.org/10.1016/j.gca.2011.02.010

Zeebe, R.E., Ridgwell, A. and Zachos, J.C. (2016) Anthropogenic carbon release rate unprecedented during the past 66 million years. *Nature Geoscience* 9, 325-329, https://doi.org/10.1038/ngeo2681

Zhang, R. (2008) Coherent surface-subsurface fingerprint of the Atlantic meridional overturning circulation. *Geophysical Research Letters* 35, https://doi.org/10.1029/2008GL035463

Figure captions

Figure 1. Changes (Δ) in bottom-water (**a**) temperature (ΔT), (**b**) practical salinity (ΔS_P), (**c**) dissolved inorganic carbon concentration (ΔDIC), (**d**) total alkalinity (ΔTA), (**e**) soluble reactive phosphate concentration ($\Delta[SRP]$), (**f**) dissolved inorganic silica concentration ($\Delta[dSi]$), (**g**) bottom-current speed (ΔU) and (**h**) calcite flux to the seafloor (ΔF) between the first 30 years (2006-2035) and the last 30 years (2071-2100) of the CMIP5 model mean, under the RCP8.5 scenario. Each map is associated with an adjacent plot that shows the annual mean of the globally averaged variables for the CMIP5 model mean (black dashed line), ESM2M (orange line), HadGEM2 (pink line) and IPSL (red line) between 2006 and 2100. Qualitative results from Mann-Kendall trend tests [*Kendall*, 1975; *Mann*, 1945] performed on the globally averaged CMIP5 model mean values between 2006 and 2100 are also shown. This test identifies whether there is a consistently increasing or decreasing monotonic trend. The sign of the trend for each

variable is depicted with green arrows for statistically significant increasing trends, red arrows for statistically significant decreasing trends, and tilde symbols for diverging trends. Statistics associated with each trend test are reported in Table S1. Grey-shaded regions are areas where models disagree regarding the sign of the trend.

Figure 2. CMIP5 model mean (**a**) calcite dissolution rate (r) at the sediment-water interface averaged between 2071 and 2100 and (**b**) change in the dissolution rate (Δr) between the first 30 years and the last 30 years of the 21st century.

Figure 3. (**a**) CMIP5 model mean temporal evolution of the global-averaged benthic dissolution rate anomaly relative to 2006 (Δr) and the respective contributions of U (light blue), DIC (red), TA (yellow) and F (dark blue) to the dissolution rate anomaly. Respective contributions of each variable were estimated by computing the dissolution rate through time when all variables are kept constant throughout the 21st century, except for the variable whose contribution is to be quantified. (**b**) Geographical distribution of the primary driver of the benthic dissolution rate, i.e., variables with the highest correlation coefficient (R^2) resulting from a multiple multivariate linear regression of r against U, DIC, TA and F.

Figure 4. (**a**) Dissolution rates from *Dunne et al.* [2012], which we term F_{dis}. The F_{dis} values from *Dunne et al.* [2012] were computed by subtracting their final modelled calcite burial flux from their final modelled calcite bottom flux. Hence, F_{dis} does not necessarily represents the dissolution rate of calcite at the sediment-water interface, but rather the fraction of the calcite flux to the bottom that is being dissolved either at the sediment-water interface or within the sediment porewaters. (**b**) Scatter plot that compares r values from this study with F_{dis} values from *Dunne et al*. [2012]. The flux of organic carbon to the bottom is taken from *Dunne et al*. [2012]. The correlation coefficient (R^2) describing the agreement between r and F_{dis} values are also shown.

Figure 5. Inter-comparison of the resolved bottom-current speed response of six Earth System and climate models to atmospheric pCO_2 accumulation. (**a**) World-averaged, resolved bottom-current speed changes relative to the beginning of the simulation, as a function of relative change to atmospheric pCO_2 for bottom waters deeper than 1 km and between 60°S and 60°N. $pCO_{2\ initial}$ is the world-averaged atmospheric pCO_2 for the first year of each simulation. pCO_2 values for the models under the RCP8.5 scenario are taken from *Meinshausen et al*. [2011]. The solid lines represent running averages over a 5-year period. Mann-Kendall trend test [*Kendall*, 1975; *Mann*, 1945] results for each of the model output are shown in Table S2. The dashed black line indicates the baseline. (**b**) Sign of the bottom-current speed change between the first and the last 30 years of the six simulations. The dark blue end of the color spectrum represents a case where all six models predict a bottom-current speed decrease, whereas the dark red end indicates the case where all six models predict a bottom-current speed increase.

Figure 6. Comparison of the resolved bottom-current speeds between models and observations. (**a**) Ratio of the collocated current speed from the CMIP5 model mean to current-meter observations. (**b**) Bottom-current speeds averaged over 378 current-meter locations deeper than 1 km in the three CMIP5 models, three CM2-O models and four configurations of the HYCOM model (see section 5.2 for description of the models) as a function of the model resolution. The black, thick line represents the current-meter average. For simplicity, the CMIP5 models are considered to be of 1° x 1° resolution.

Figure 7. (**Left column**) Histograms of the distribution of resolved bottom-current speeds corresponding to the 378 current-meter sites deeper than 1 km. Lines represent kernel density functions. (**Right column**) Correlation diagrams between measured bottom-current speeds and model-simulated values. Both the current meter measurements and model predictions do not include tides. Correlation coefficients (R^2) are shown for each model.

Figure 8. Global seafloor calcite dissolution rate as a function of time, simulated by the CMIP5 model mean under the RCP8.5 scenario (black line), accounting for the uncertainties associated with each CMIP5 model mean variable (CMIP5-intermodel spread) and their propagation into the computed dissolution rates (grey shaded area).

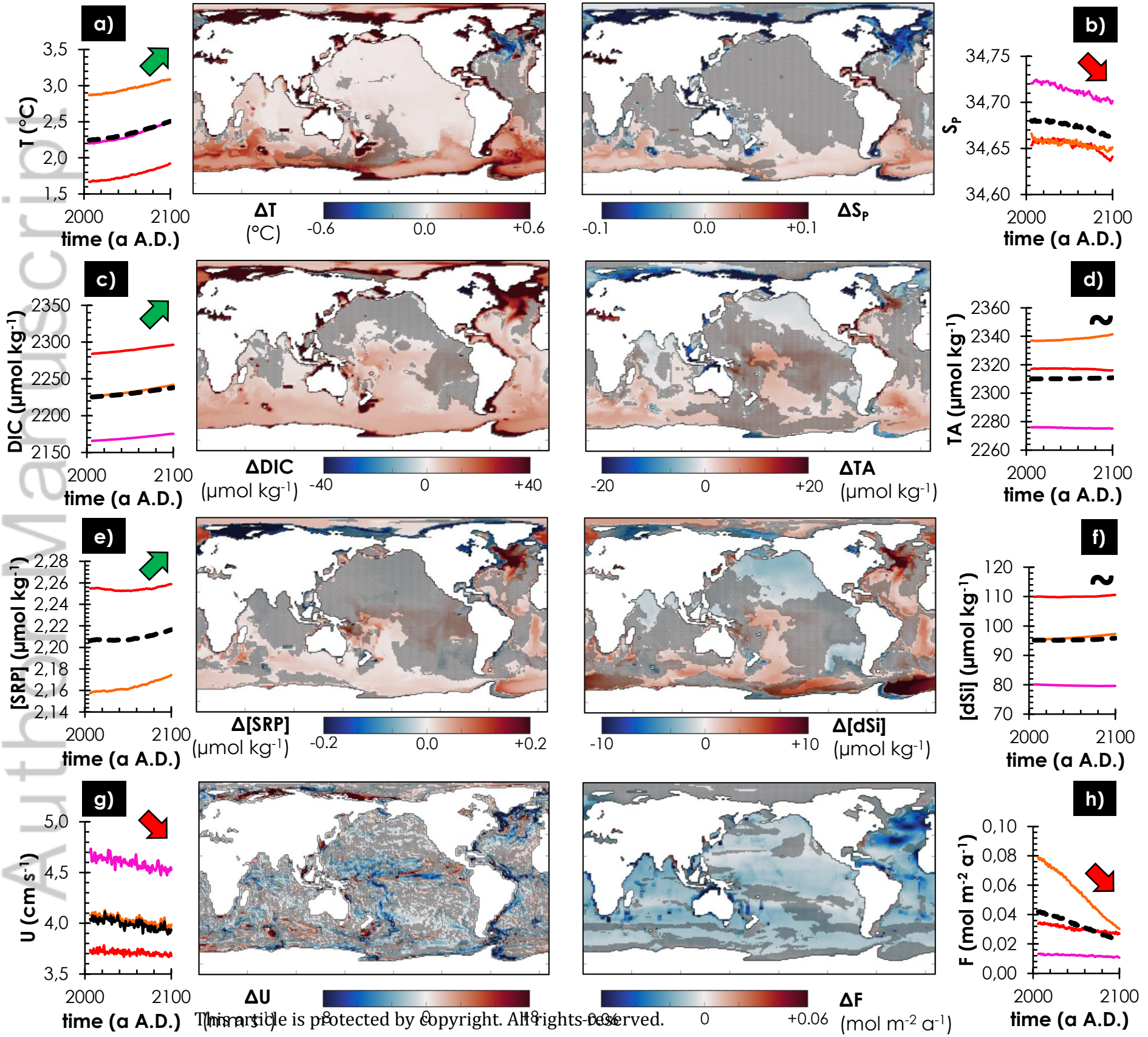

a) r averaged between 2071 and 2100

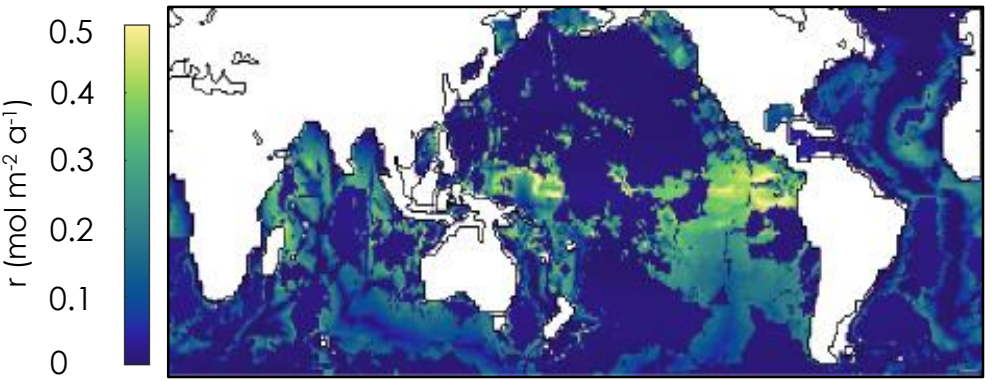

b) 21st century r change

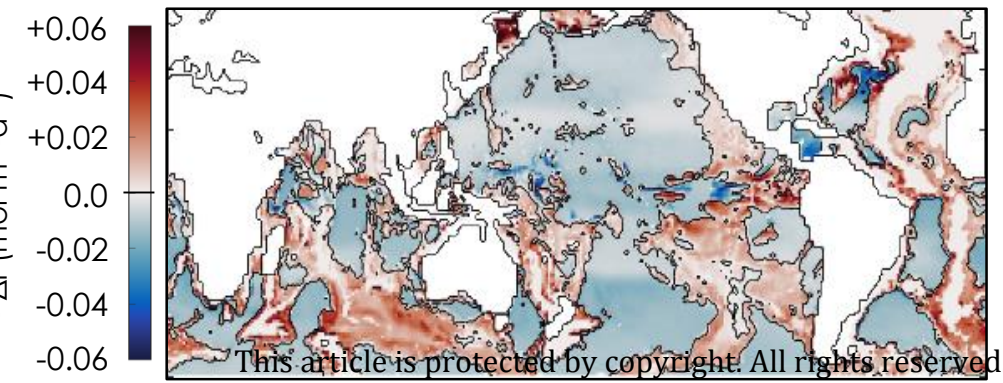

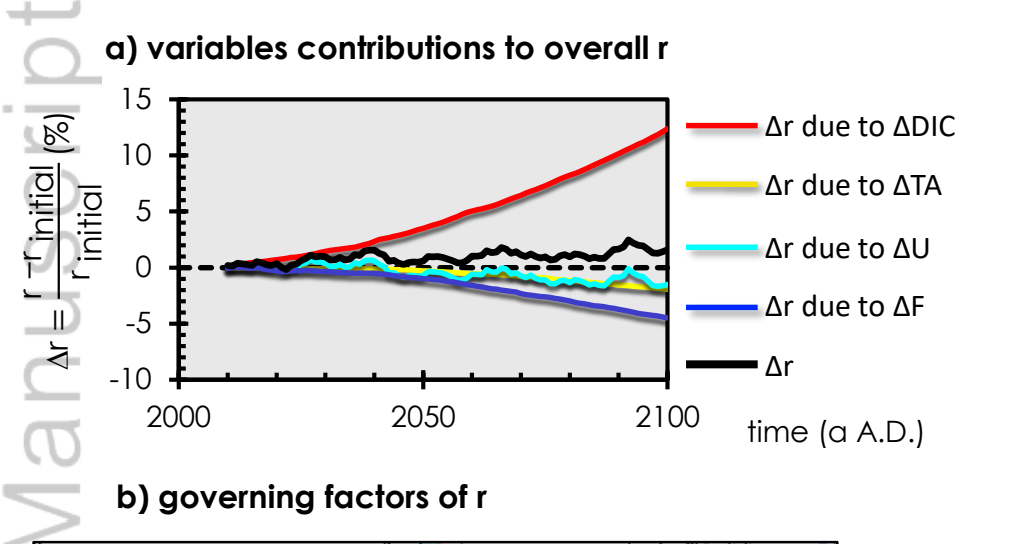

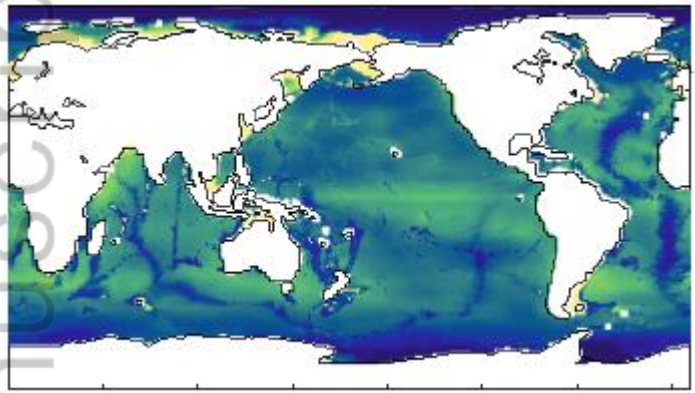

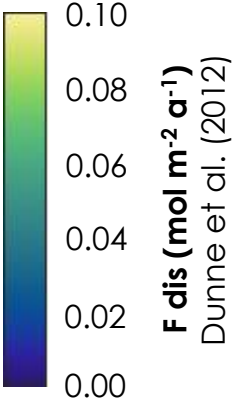

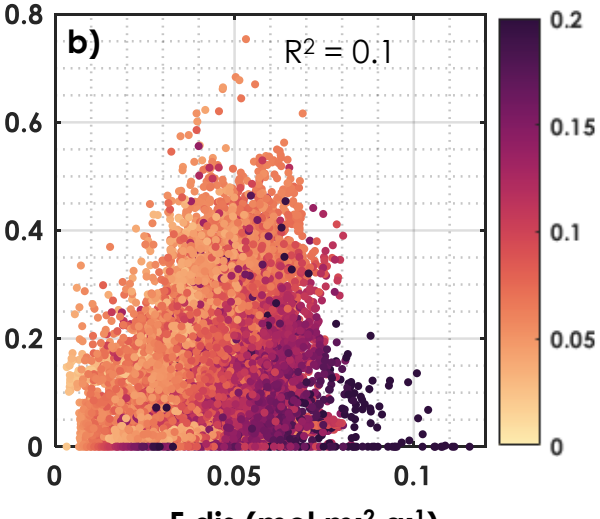

r (mol m-2 a-1)
This study, 2006-2035